Final Report – BETO

Award Number: EE0007984

Multitude Characterization and Prediction of DOE Advanced Biofuels Properties

PI

Dr. Kareem Ahmed

University of Central Florida

The Center for Advanced Turbomachinery & Energy Research

U.S. Department of Energy

Office of the Biomass Program

ACKNOWLEDGEMENT:

This material is based upon work supported by the U.S. Department of Energy's Office of Energy Efficiency and Renewable Energy (EERE) under the Bioenergy Technologies Office (BETO) Award Number DE-EE0007984.

Multitude Characterization and Prediction of DOE Advanced Biofuels Properties

A. Summary/Abstract

Advanced multitude of experiments ranging from the liquid fuel to combustion are conducted on Co-OPTIMA fuels to aid the characterization of the fuels. The series of targeted experiments characterized Co-OPTIMA fuel spray atomization, flame topology, flame speed, autoignition, volatility, viscosity, soot/coking, and compatibility. The fuels are selected and prioritized based on input from national lab members. The research characterized and predicted biomass-based, low greenhouse gas fuels and blends combustion, autoignition, and physical properties of mixtures of identified compounds at engine-relevant conditions, in particular those properties that blend non-linearly.

The main challenge of Co-OPTIMA is the evaluation of a variety of biofuels and blends in all the reaction conditions that might be encountered in new high-efficiency engines. Despite the improved high-throughput experimental techniques, it seems unlikely that all of the performance metrics could be measured for all relevant petroleum derived, bio-derived molecules and mixtures, and reaction conditions. A series of targeted experiments ranging from the liquid fuel to the combustion process is required, and to extract the maximum information from each experiment. These targeted experiments evaluated how a specific fuel will perform in an engine. The series of targeted experiments are as follows:

(a) Spray Atomization, Vaporization and Droplet Formation
(b) Combustion Flame and Local Fuel/Air Image-Based Measurements
(c) Laminar Flame Speed Measurements
(d) Autoignition and Soot Measurements
(e) Synchrotron Coupled Fundamental Autoignition Experiments
(f) Fuel Coking and Hot Surface Deposit
(g) Fuel Volatility Measurements
(h) Viscosity Measurements
(i) Seal Flexible Fuel Compatibility

These experimental processes provide an essential pathway for the prediction of fuel behaviors in engines and systematic process for fuel down select.

B. Project Objectives

The goal of this project is to provide a detailed data set of multiple combustion experiments relevant to engine combustion of Co-Optima fuels.

The product that will result from this project is data and information for the fuel behavior that mitigates the sensitivity of the alternative fuels. This characterization process will mitigate the potential for combustion operability issues due to the particular fuel being used at a specific time. This process of fuel characterization and property prediction has applications in both selection of Co-Optima fuels and optimization of the fuels. The primary initial objective is to develop a data matrix that can be utilized in the selection process of the biofuels and blends. The basic concept can then be extended to optimize a wide variety of other fuels.

At the conclusion of the project, we expect to have validated fuel characteristics and properties and quantified uncertainty levels that can be applied to select and optimize fuels. In addition to physical designs and test data, we expect to have easy-to-apply performance correlations that will aid designers in the application and operation of the Co-Optima fuels.

C. Technical Scope Summary

This project is focused on the challenge of providing experimental fuel characterization and property prediction for Co-Optima biofuels and blends. A series of targeted experiments will characterize and predict Co-Optima fuel spray atomization, flame topology, flame speed, soot induction time, volatility, viscosity, soot/coking, and compatibility. Fuels will be selected and prioritized based on input from national lab members. The research will characterize and predict combustion, autoignition, and physical properties of mixtures of identified biomass-based fuels at engine-relevant conditions, in particular those properties that blend non-linearly.

The technical approach includes

1. fuel test matrix development based on known fuel properties and with the objective of optimizing the experimental plan to allow testing to be conducted as efficiently as possible. This will also reduce experimental uncertainty by allowing fuels with requiring similar instrument set up and calibration to be tested together;
2. execution of a spectrum of fuel characterization experiments from fluid-to-combustion; and
3. correlation of molecular structure with fuel properties derived from the experimental data.

The project will be conducted in two budget periods:

The fuels will be segregated in to two groups (group 1 and 2) - each with approximately five promising fuels. This grouping will be conducted in close collaboration with the National Lab projects to synchronize the effort. The fuel group 1 will be tested in the first budget period and fuel group 2 in the second budget period.

Budget Period 1: Fuel matrix development, experimental plan optimization and fuel characterization experiments for fuel Group 1

Budget Period 2: Fuel matrix development, experimental plan optimization and fuel characterization experiments for fuel Group 2

D. Tasks To Be Performed

The research is focused on characterization of Co-Optima fuels. We will coordinate with National Labs on the selection of fuels required for characterization. The work on the project is organized into the following tasks:

- **Task 1.** Fuel matrix development and experimental plan optimization (First 4-months in yr 1)
  Select fuels for each of the detailed characterization experiments (task 2) in consultation with the National Labs. The fuel matrix development process will be based on composition, known properties, preliminary property information from the National Labs, comparison of fuel characteristics with those of current engine fuels. A fuel matrix will be made up of fuels with similar properties in order to optimize experimental resources. For example, for several of the spectrum of fuel characterization experiments to be performed in Task 2 the experimental set up and calibration must be modified for high reactivity versus low

reactivity fuels, or fuels with diesel-like volatility versus gasoline-like volatility. By combining fuels into a series of test matrices of similar fuels we can reduce experimental uncertainty and optimize the use of experimental resources.

- **Task 2.** Execution of a spectrum of fuel characterization experiments (fluid-to-combustion) (30 months over yr 1 to yr 3)

  Conduct a series of targeted experiments with well quantified uncertainties ranging from the liquid fuel to combustion on selected fuels to compliment the modeling teams. The series of targeted experiments will characterize and predict fuel spray atomization, flame topology, flame speed, induction time, volatility, viscosity, coking/deposits, and compatibility. Fuel candidates selected from Task 1 will be distributed among the following subtasks based on discussions with National Labs and experimental availability. The fuels will be segregated in two or more groups (from task 1). The experiments will be conducted in sub-tasks. The sub-tasks will evaluate the fuels in series and parallel based on the grouping of the sub-task experiments. For the first budget period, the group 1 fuels will be evaluated for each experiment (sub-tasks) in series; however, four experimental sub-tasks will be conducted in parallel for a duration of approximately 8-months and then the other four experimental sub-tasks will be conducted in parallel for a duration of approximately 8-months. The schedule is defined by resources and manpower availability. The task will be revisited to characterize and evaluate fuel grouping 2 in budget period 2.

  - Task 2.1 Spray Atomization, Vaporization and Droplet Formation (8-months in yr1 and 8-months in yr2-3)

    The research will focus on understanding the fuels spray break-up, atomization, mixing and combustion of relevance to combustion engines. Detailed imaging of fuel spray dynamics using structured light-field focusing which is a novel diagnostic technique to image the core spray jet dynamics in an extreme, high optical density fuel spray. Furthermore, droplet size from the spray will be simultaneously measured. The experiment will characterize fuel spray injection, atomization, and mixing to increase engine efficiency. From the data analysis, the key parameters (e.g., spray angle) will be identified and a regression model developed that predicts the fuel behaviors within 20% uncertainty.

  - Task 2.2 Combustion Flame and Local Fuel/Air Image-Based Measurements (8-months in yr1-2 and 8-months in yr3)

    This subtask will provide a detailed analysis of the fuel injector spray, fuel-air distribution and combustion at various high pressure fuel conditions to optimize for homogenous fuel mixing and clean combustion. The measurements will be composed of spray-flame combustion testing in a high-pressure, optically accessible DI combustion chamber. The optically accessible chamber is reminiscent of IC engines for detail measurements. The spray fuel injection and fuel/air will be characterized to enhance engine efficiency. Turbulence induction in combustion chambers will tailored to increase flame speeds resulting in higher burning rate and enhance efficiencies by 70%. Furthermore, local optical fuel/air spatio-temporal measurement using C2/CH florescence imaging technique inside the optical access constant volume combustion chamber. The specifics of the chamber: charge pressure 1 - 20 bar, combustion pressure 1 - 130 bar, Gaseous and Liquid Fuels (premixed or stratified), pre-heating temp. 30 - 130ºC, fuel injection pressure 103 bar, instrumented with optical access.

The measurement will demonstrate fuel-air correlation function relative to florescence intensity within 15% of the expected values.

- Task 2.3 Laminar Flame Speed Measurements (11-months in yr1-2 and 11-months in yr2-3)

Laminar Burning Velocity (LBV) is an important fundamental property of a fuel/air mixture and it depends on the composition, temperature, and pressure. Therefore, the knowledge of the dependence of the laminar burning velocity on above mentioned parameters can be used to design advanced engines as LBV can affect efficiency and heat release rates. We will measure burning velocities in UCF's heated (up to 1100K), high initial pressure (1-10 bar) spherical flame chamber using high-speed visualization and pressure measurements. Flame radius as a function of time and burning velocity data will be obtained from post-processing and numerical analysis of the Schlieren images as well as the pressure data. Fuels and blends will be selected in consultation with national lab. The objective will be to measure LBV with a maximum uncertainty of 10%.

- Task 2.4 Soot Volume Fraction and Induction Time Measurements (5-months in yr2 and 5-months in yr3)

Experiments will be performed using shock tube and laser extinction methods to investigate various oxygenated systems under engine-relevant conditions. Soot induction times and soot volume fraction will be measured in this study. Soot-induced laser light extinction at 633 nm and the light emission by soot particles at 670 nm will be measured. Fuel candidates will be chosen in consultation with National Labs so that it will be possible to get information such as, what is the effect of branching, double bonds, and functional groups position on emissions. We plan to conduct these experiments for various pressures from 1 to 20 atm and temperatures from 1500 to 2000 K for different fuel/oxidizer combinations.

- Task 2.5 Synchrotron Coupled Fundamental auto-ignition Experiments (2-months in yr2 and 2-months in yr3)

The details of the combustion chemistry are important in determining fuel efficiency, pollutant formation, and health and safety effects of combustion byproducts. Tunable, high brightness radiation in the vacuum ultraviolet, as provided by beam line 9.0.2 from the Advanced Light Source (ALS) located at Lawrence Berkeley Lab (LBNL), allows isomer-specific photoionization detection of reactants and products from gas-phase reactions. We will apply a highly-multiplexed experiment, monitoring all products with superior sensitivity, to isomer-resolved study of reactions and molecules that are of fundamental scientific interest and are important in the formation of soot, hydrocarbon oxidation and autoignition chemistry. This work will be conducted in collaboration with the Air Force Research Lab facility (AFRL, Edwards, CA) using available reactors (jet stirred reactor, flow reactor, etc.). Both reactors can operate in the temperature range from 300-800K, however, the choice of the reactor will be based on other ongoing work at ALS. The schedule for this work will be finalized in consultation with AFRL and ALS and may happen sooner than projected at this time.

- Task 2.6 Cylinder Carbon Deposit (8-months in yr1 and 8-months in yr2-3)

Exposure of hydrocarbons to hot metal surfaces can produce carbonaceous deposits on engine components over time. The rate of deposit formation depends on the nature of metal surfaces in the fuel systems and gasoline additives used to inhibit solid

deposition. These deposits adversely affect an engines operation and performance. Furthermore, these deposits taken up into the engine oil decrease oil lifetime. Our experiment can be used as the simplest form of a cylinder with better control over hot surfaces and surface composition. In previous work we have examined the formation of these deposits in bio-derived fuel pumped through hot (325˚C) tubing at 600 psi. In this effort, hot tube and liquid impingement will be used to assess the thermal stability of the Co-Optima fuels. An identification of compositional parameters that relates to the amount of carbon deposition will be defined. The composition will be quantified in terms of micro-g per cm^2.

- Task 2.7 Fuel Volatility Measurements (8-months in yr1-2 and 8-months in yr3)

ASTM methods will be used for fractional distillation of fuels. By fractionating the fuels we will thoroughly understand the volatility of a given fuel. In addition, each fraction will be analyzed by gas-chromatograph mass-spec (GC-MS) to correlate it chemical composition to the volatility data. The important information to get is the compositional data of the fuel fractions. Without this information we will not be able to make composition/combustion correlations. This is a foundation of all the work. It's critical we gather the information internally for the correlation of molecular structure.

- Task 2.8 Viscosity Measurements (8-months in yr1 and 8-months in yr2-3)

Viscosity measurement fixture will be used to test biofuels and blends selected in consultation with the National Labs. This fixture will consist of a quartz crystal microbalance (QCM) in a sealed unit to measure viscosity from 20˚C to 200˚C. There is a linear relationship between the QCM frequency and the square root of the density-viscosity product of the liquid: $\Delta f = k\Delta\sqrt{\rho\eta}$*. The viscosity measurements will be demonstrated within a 5% uncertainty.*

- Task 2.9 Seal Flexible Fuel Compatibility (8-months in yr1-2 and 8-months in yr3)

A problem occurring with prolonged exposure of polymers to fuels is the degradation of these polymers. This is problematic for polymers used in o-rings and other polymers utilized in other components exposed to fuel. We have investigated the long-term effect of fuels such as ethanol and bio-derived jet fuels on Buna-N O-rings. All of these biofuels caused the o-rings to shrink. Addition of a bio-derived aromatic compound at as little as 1% improved the seal swell characteristics. We will perform similar studies with the Co-Optima drop in fuels. O-ring samples representative of fuel system will be tested: Nitrile, fluorocarbon and fluorosilicone o-rings. Mass and volume measurements at 0, 9 and 28 days will be conducted. We will quantify Volume changes as that would correlate with seal swell within a 10% of expected values.

- **Task 3.** Correlation of molecular structure (4-months in yr2 and 6-months in yr3)

Under this task, the molecular structure relationships to observed measurements will be developed based on statistical analysis. The correlation of the molecular structures will be beneficial to identify fuel similarities. The goal is to examine the relationship between the experimental results and the fuel molecular structure. The approach will be based on statistical analysis. The information will be compared to the initial assumptions made in selection and fuel grouping process in Task 1. This will contribute to the evaluation of the selection process established in Task 1 and contribute to the go/no-go decision for the selection process considered in Task 1.

Table 1: Project Schedule

Table 1. Project Schedule																																				
Tasks	Month After Award																																			
	1	2	3	4	5	6	7	8	9	10	11	12	13	14	15	16	17	18	19	20	21	22	23	24	25	26	27	28	29	30	31	32	33	34	35	36
1. Fuel matrix development and experimental optimization	■	■	■	■															■	■																
2. Execution of a spectrum of fuel characterization experiments				■	■	■	■	■	■	■	■	■	■	■	■	■	■	■	■	■	■	■	■	■	■	■	■	■	■	■	■	■	■	■		
2.1 Spray Atomization, Vaporization and Droplet Formation				■	■	■	■	■	■	■	■								■	■	■	■	■	■	■	■										
2.2 Combustion Flame and Local Fuel/Air Image-Based Measurements											■	■	■	■	■	■	■	■									■	■	■	■	■	■	■	■		
2.3 Laminar Flame Speed Measurements				■	■	■	■	■	■	■	■	■	■	■					■	■	■	■	■	■	■	■	■	■	■							
2.4 Soot Volume Fraction and Induction Time Measurements														■	■	■	■	■												■	■	■	■	■		
2.5 Synchrotron Coupled Fundamental Autoignition Experiments																	■	■												■	■					
2.6 Fuel Coking and Hot Surface Deposit				■	■	■	■	■	■	■	■								■	■	■	■	■	■	■	■										
2.7 Fuel Volatility Measurements											■	■	■	■	■	■	■	■									■	■	■	■	■	■	■	■		
2.8 Viscosity Measurements				■	■	■	■	■	■	■	■								■	■	■	■	■	■	■	■										
2.9 Seal Flexible Fuel Compatibility											■	■	■	■	■	■	■	■									■	■	■	■	■	■	■	■		
3. Correlation of molecular structure															■	■	■	■													■	■	■	■	■	■
4. Manage and Report	■	■	■	■	■	■	■	■	■	■	■	■	■	■	■	■	■	■	■	■	■	■	■	■	■	■	■	■	■	■	■	■	■	■	■	■
- Kickoff Meeting	♦																																			
- Progress Reports		♦			♦			♦				♦				♦				♦				♦				♦				♦			♦	
- Final Results Meeting																																			♦	
- Final Report																																				♦

Task number: 1

The fuel selection went through an iterative process where we devised a list of a broad spectrum of fuels that are compatible with the experiments and shared it with the national labs. We first selected a set of fuels from the DOE list that give a broad variation (ether, normal alkane, branched alkane, cyclic alkane, and alcohol). The fuels were checked for the compatibility with the experiments. We shared the list with Bob McCormick which then involved Anthe George (LBL) Gina Fioroni (NREL) in the discussion. Bob had concerns for flashing and freezing points for some of the fuels and made alternate suggestions for fuels. We then took the alternate suggested fuels and devised a new list of potential fuels that is based on fuel availability and compatibility with the experiments. Then we followed up with Bob, Anthe, Gina, with the revised list. We agreed on two fuels but the other three fuels more information about boiling, flash, freezing, CN information was needed. We provided that information and revised the list further with a new list where we came to agreement with 3 fuels and still 2 remaining to cover the spectrum. Dr. Subith Vasu attended the SAE Congress meeting and discussed the fuels with the Co-Optima team at the meeting and came back with a list of key candidates. We discussed a new revised list with Bob and we were in agreement on the fuel list except for one fuel which could not source commercially

available (farnesane 2,6,10 trimethyl dodecane). Bob reached out to Amyris which has agreed to give us a couple of drums of farnesane shipped from Brazil to NREL. They will send us two 5 gal cans. Note the fuels are all bio-derived fuels.

Thus UCF's fuel matrix 1 has the following 5 compounds for the study:

1- Ethanol (alcohol)
2- Diisobutylene (alkene)
3- Methyl furan (furan)
4- Cyclopentanone (ketone)
5- Methyl acetate (ester)

Thus UCF's fuel matrix 2 has the following 5 compounds for the study:

1- Ethers - dibutoxymethane (ether)
2- dodecane (normal alkane)
3- farnesane 2,6,10 trimethyl dodecane
4- butyl cyclohexane (cyclic alakne)
5- 2-Nonanol (alcohol)

Task number: 2

The sub-tasks that are conducted are the following:

Task 2.1 Spray Atomization, Vaporization and Droplet Formation

Introduction:

The study of atomization is a critical process in determining the performance of combustion engines. The effectiveness of atomization controls **air-fuel mixing, combustion efficiency, pollutant emissions and stability**. The quality of atomization in this study will be compared to each fuel via the quantification of macroscopic and microscopic characteristics. The dominant macroscopic characteristics of spray development are spray tip penetration and spray cone angle. Spray cone angle is the angle formed by two straight lines drawn from the injector orifice tangent to the spray to a specified downstream distance of the injector. This downstream distance is usually a function of the penetration length or a function of the nozzle diameter [1]–[3].Spray tip penetration is defined as the distance from the nozzle tip of the injector to the farthest spray tip. Essentially the spray cone angle and spray tip penetration are important parameters that help understand the spray's global characteristics. Direct imaging of sprays and the evaluation of the

spray angle and penetration provides useful information about the global air entrainment in sprays and thus provides an indication of fuel-air mixing and vaporization.

Subsequent to macroscopic characteristics, microscopic characteristics important to atomization are droplet size diameters and Sauter Mean Diameter. It is known that spray characteristics plays an important role from the viewpoint of thermodynamic performance and pollutant emissions in the combustion phenomena. A typical example is a combustion engine requires a middle ground between the number of small droplets needed to cold start an engine and the number of large droplets needed to control the flame stability. An accurate evaluation of droplet size and its distribution provides the capability to develop evaporation models and predict spray evolution. Sauter Mean Diameter or SMD is another parameter that is extremely important within the combustion community and is extensively used in the characterization of gas liquid or liquid liquid dispersions[4]. The SMD is the ratio of total droplet volume to the total droplet surface area, this value reflects both the evaporation rate and energy content of the spray and is crucial to the understanding of atomization in combustion applications.

In this study five different biofuels were studied, each of these biofuel were blended at 30% volume percentage with certified Diesel. The biofuels are Butylcyclohexane, Dodecane, Dodecane with isomers, Formaldehyde dibutyl Acetyl and Nonanol.

Experimental Approach: Spray cone angle and tip penetration.

The objective of this study is to measure the spray cone angle and tip penetration. This is done by setting up a high speed imaging device, recording at 10,000 FPS 143 μm/pixel, a fixed distance from the flat tip orifice injector opening. A multi-hole injector similar to ones used in IC engine was used for this study. The experimental setup is shown in Figure 1 and Figure 2; which consist of: (i) a Photron FastCAm; (ii) a pulse generator; (iii) an Engine Control Unit (ECU); (iv) fuel reservoir; (v) fuel injector; (vi) DC power supply; (vii) Haskel AW-B22 fuel pump; (viii) an continuous wave Nd:YAG laser; and an (ix) optics system. Before each experiment, the camera came on 0.04 ns before the first injector pulse. The pulse width of the injector was set at 50 ms, with a single period being 100 ms, and allowed to run for one second, into an environment at 70°F and 101.32 KPa and the Fuel injector line pressure was set to 1450±36.7 psi.

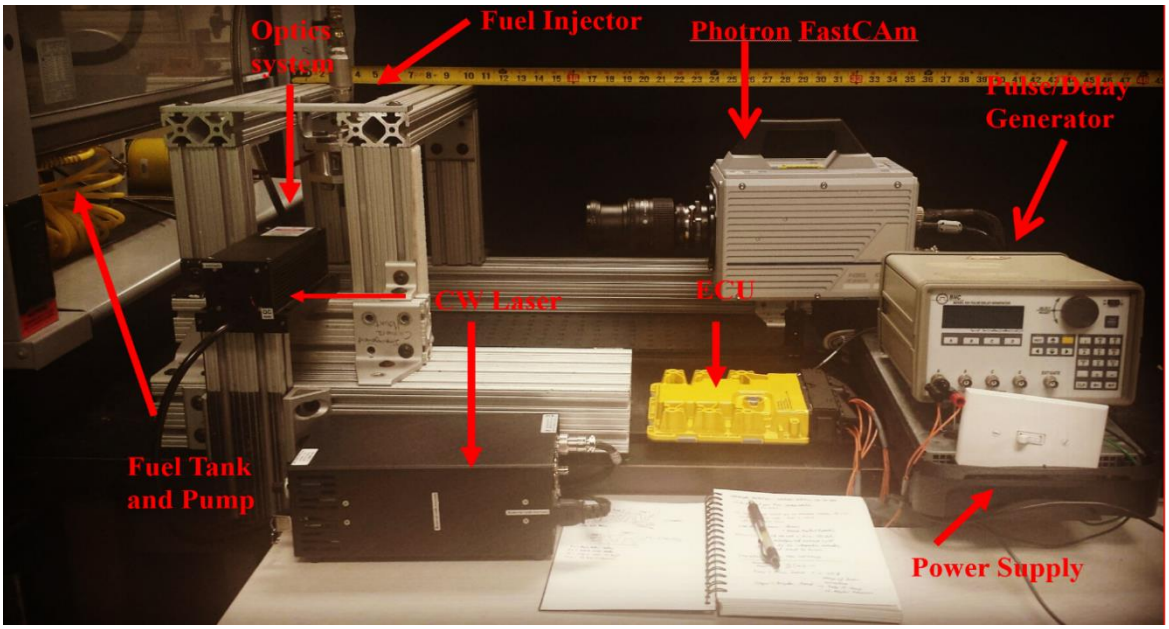

Figure 1: Spray Cone Angle and tip penetration apparatus layout

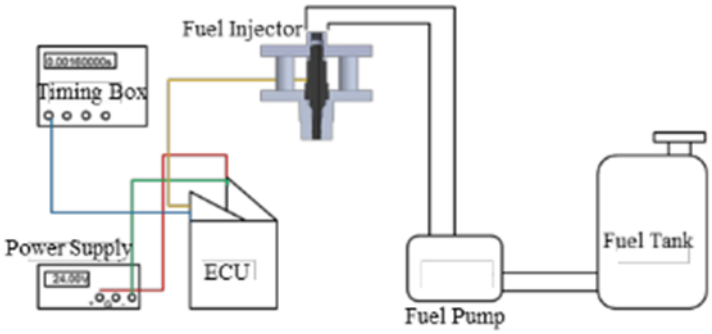

Figure 2:Fuel injector control diagram

To calculate the spray cone angle, a point is taken on the diffuse boundary of the edge cone away from the nozzle and a line is drawn directly from that point to the nozzle edge on the corresponding side. The images acquired from the set was corrected for background noise, then each image were binarized using an adaptive thresholding technique which chooses a threshold based on the local mean intensity in the neighborhood of each pixel. The images were then calculated for its cone angle. The method implemented is a typical method applied in the spray community ,it is based on measuring the angle between two lines interpolated to the spray edges, where a least-square technique is used to determine the best fit of these lines. The lines extend from the spray's origin to a downstream distance relative to the spray penetration length. The lines origin is fixed from the tip of the injector nozzle. The penetration length up to which the interpolated lines are fitted varies between publications, but it is typically between 50% to 60%. These percentage are common due to the fact that at these percentages the spray leading edge does not have an effect on the cone angle[6]-[9]. In fact, it was found by Pastor et al. that at 45%, 50% and 60% penetration length spray cone angles do not change significantly. Spray tip penetration was calculated by tracing the

binarized image using bwboundaries function. The maximum penetration point was then extracted from the trace coordinates. The macroscopic characteristics of the spray was analyzed at exactly 2.1 millisecond. Figure 3 portrays the image processing method used.

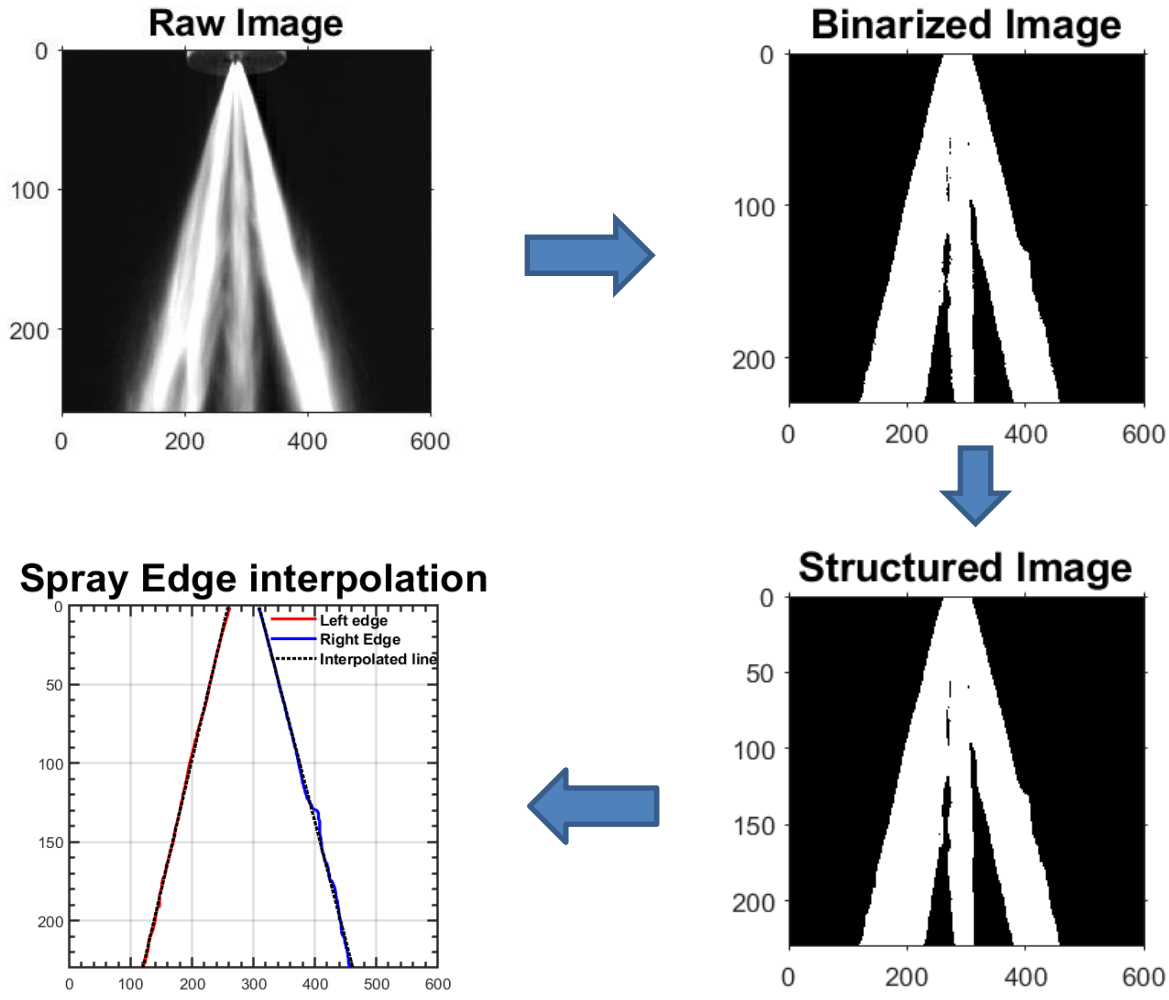

Figure 3:Image Processing Method

Results:

The experimental method conducted was done to be applicable to the standards outlined by the Yokota and Matsuoka equations, (eq. 1) and (eq. 2) where the ***spray cone angle θ***, is a function of: ***the Liquid Phase Reynolds Number*** Re_L, ***orifice opening*** d_o, ***injector length l, density of the liquid*** ρ_L, ***density of the air*** ρ_A, and ***a correction factor n***. Theoretical and experimental findings were found to be within a reasonable range to prove validation [3]. With a pressure of 1450±36.7 PSI, the percent difference between certified gasoline theoretical fittings and experimental findings was 3.88% where the theoretical angle was 8.04°, and for the experimental findings 7.73±0.142°. Thus, this validates the method used to extract spray cone angle.

$$\theta = 0.067 Re_L^{0.64} \left(\frac{l}{d_o}\right)^{-n} \left[1 - e^{\left(0.023 \frac{\rho_L}{\rho_A}\right)}\right]^{-1} \quad \text{(eq. 1)}$$

$$n = 0.0284 \left(\frac{\rho_L}{\rho_A}\right)^{0.39} \quad \text{(eq. 2)}$$

The spray cone angle in a fuel injector is generally regarded as a function of various parameters including fuel viscosity, fuel density, temperature, pressure, injector diameter and injector length. In this experiment the pressure, temperature, and injector size were held constant. Data obtained from the spray cone and spray penetration experiments are presented in Presented in figure 4 and 5. The sample size of each fuel was 30. Figure 6 compares average spray dispersion of each fuel. It can be observed from this figure the dispersion of the spray closely matches the quantitative value of the measured spray cone angle.

Fuel Blend	**Cone angle**
Butylcyclohexane 30%	$66.48 \pm 0.52°$
Dodecane 30%	$67.35 \pm 0.43°$
Dodecane with isomers 30%	$66.79 \pm 0.49°$
Formaldehyde Dibutyl Acetyl 30%	$66.75 \pm 0.58°$
Nonanol 30%	$67.99 \pm 1.51°$

Figure 5: Cone angle of 30% Fuel Blends

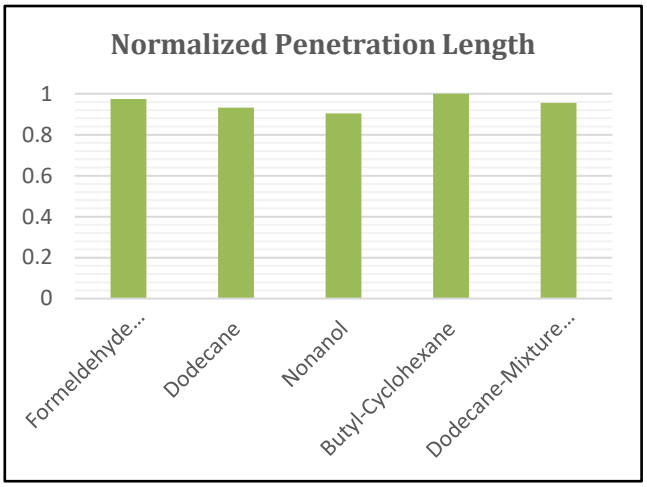

Figure 4:Penetration length of 30% Fuel Blends

The spray cone angle in a plain orifice atomizer is generally regarded as a function of various parameters including fuel viscosity, fuel density, temperature, pressure, injector diameter and injector length. In this experiment the pressure, temperature, and injector size were held constant. Data obtained from the spray cone experiments are presented in Table 2.

Table 2: Spray cone angle for each fuel blend.

Blend %	10%-vol	20%-vol	30%-vol
Methyl Acetate	$\mathbf{7.86 \pm 0.11°}$	$\mathbf{6.05 \pm 0.11°}$	$\mathbf{5.79 \pm 0.10°}$
Diisobutylene	$\mathbf{5.44 \pm 0.08°}$	$\mathbf{6.6 \pm 0.05°}$	$\mathbf{6.71 \pm 0.05°}$
Methyl Furan	$\mathbf{6.7 \pm 0.23°}$	$\mathbf{7.24 \pm 0.12°}$	$\mathbf{8.08 \pm 0.04°}$
Cyclopentanone	$\mathbf{7.81 \pm 0.18°}$	$\mathbf{7.16 \pm 0.04°}$	$\mathbf{6.97 \pm 0.09°}$
Ethyl Alcohol	$\mathbf{8.88 \pm 0.13°}$	$\mathbf{6.52 \pm 0.08°}$	$\mathbf{6.28 \pm 0.04°}$

Experimental Approach: Droplet size

The metric for microscopic characterization which contains droplet size distributions and Sauter Mean diameters will be attained via the utilization of a Particle Doppler Interferometer (PDI). The theory of operation of a PDI lies in the manipulation of light scatter to produce a difference in doppler frequency as a droplet is passing by. The difference in doppler frequency causes a fringe pattern. The spacing of the interference fringe is measured and found to be inversely proportional to the droplet diameter. Using this correlation many representative diameters can be derived. The interest in this study is the derivation of the Sauter Mean Diameter (SMD). The SMD is the ratio of total droplet volume to the total droplet surface area, this value reflects both the energy content and the evaporation rate of the spray and is critical for the understanding of atomization in combustion applications.

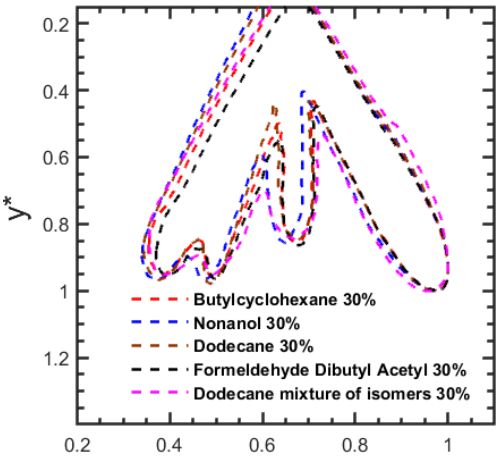

Figure 6:Spray Dispersion

Results:

In this experiment three different mean diameters were calculated using the PDI, they include D_{10}, D_{20}, D_{30} and D_{32}. D_{10} is the arithmetic mean diameter and it is best suited for calculating evaporation rates. D_{20} is surface mean diameter, this mean diameter is best suited for surface controlling applications such as absorption. D_{32} is the SMD, this diameter is best utilized to calculate the efficiency and mass transfer in chemical reactions. D_{30} is the volume mean diameter and it is typically used in hydrology. Presented below are findings for each fuel blend. The estimated size uncertainty of the PDI is **0.5%.**

Fuel Blend	$D_{10}(\mu m)$	$D_{20}(\mu m)$	$D_{30}(\mu m)$	$D_{32}(\mu m)$
Neat Diesel	1.1	1.1	1.2	1.3
30% Butylcyclohexane	1.1	1.2	1.2	1.3
30% Dodecane	1.1	1.1	1.2	1.3
30% Dodecane with Isomers	1.1	1.2	1.2	1.3
30 % Formaldehyde Dibutyl Acetyl	1.1	1.1	1.2	1.3
30% Nonanol	1.0	1.1	1.1	1.2

Table 1: Representative Diameters of Biofuel Blends

Droplet sizes regardless of fuel are strongly biased toward having a large number of "small" droplets. Droplet sizes below 0.5 mm^2 were omitted to preserve clarity of the data. However, within each fuel consideration it can be seen that there are local modes in which particle sizes may be grouped into distinct bins.

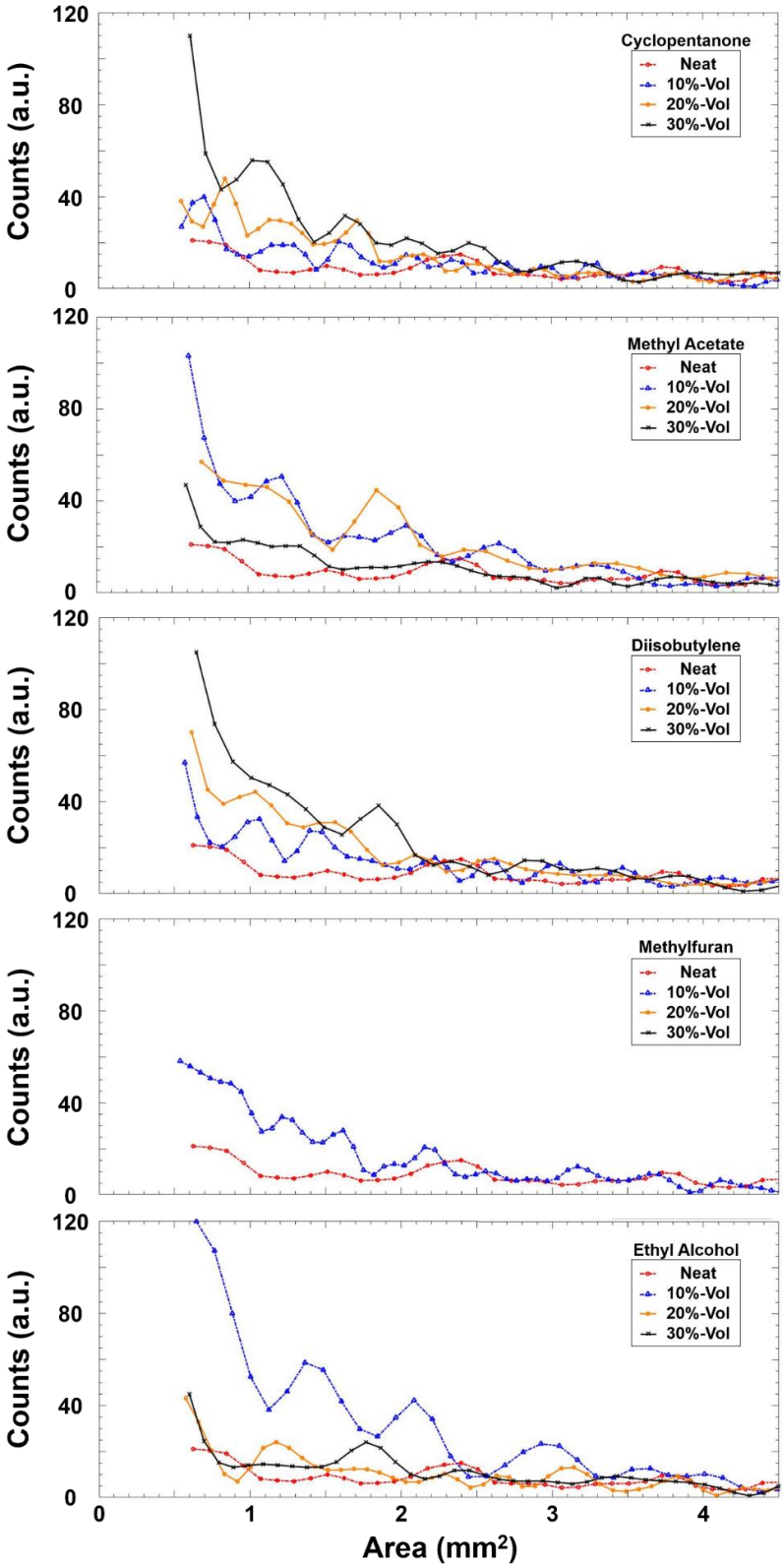

Figure 7: Droplet size distribution for each fuel, and blend considered.

Task 2.2: Combustion Flame and Local Fuel/Air Image-Based Measurements

Locally measure equivalence ratio distribution of the injector spray inhomogeneous fuel-air mixture of using C2*/CH*

Facility:

- Charge Pressure: 1 - 20 bar
- Combustion Pressure: 1 - 130 bar
- Gaseous and Liquid Fuels (premixed and non-premixed)
- Std. Deviation (Φ): 0.0072
- Pre-heating Temp: 30 - 130°C
- Fuel Injection Pressure: Up to 103 bar
- Heavily Instrumented with 6" Optical Access (Dyn. Press, FAR, Temp)

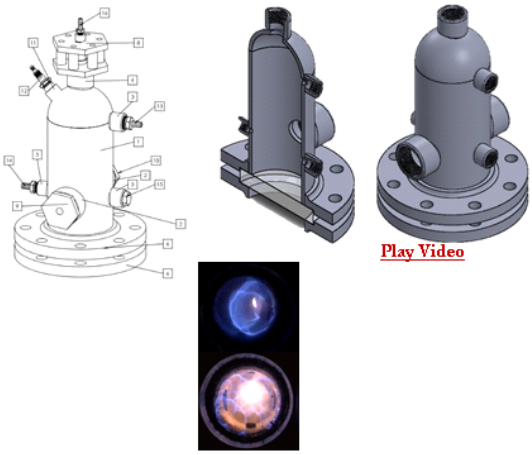

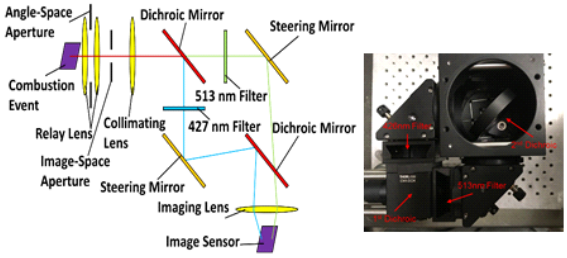

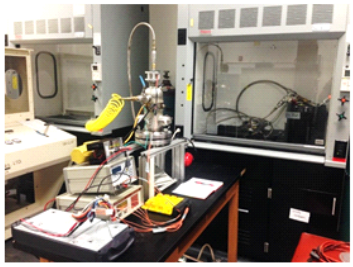

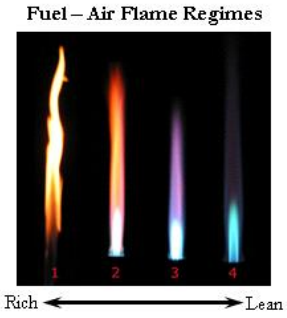

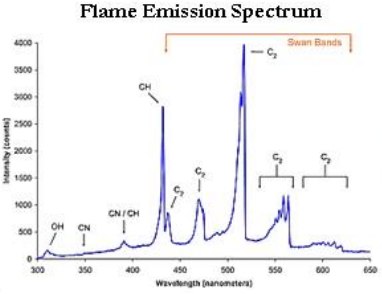

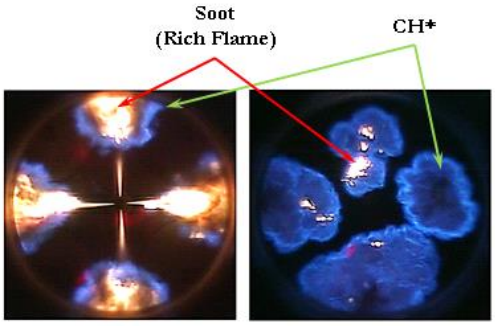

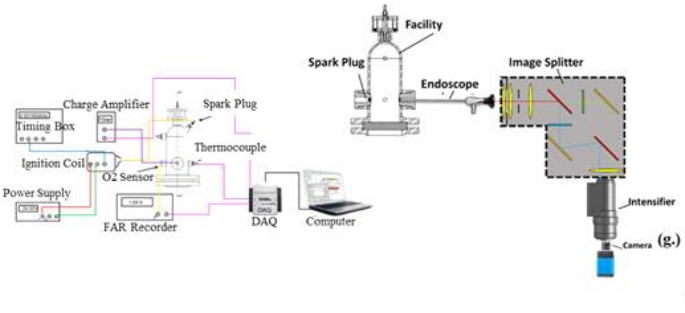

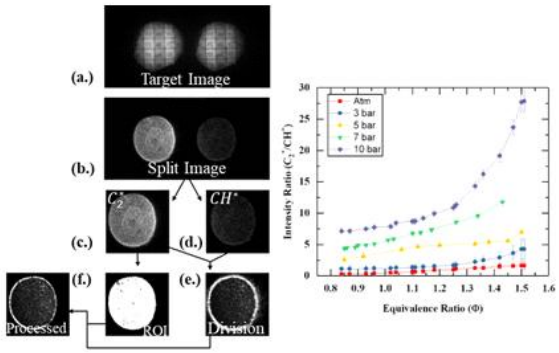

The following section presents results associated with local fuel-air distribution attained via line of sight chemiluminescence imaging of various biofuel mixtures. The apparatus associated with capturing local fuel-air measurements is illustrated in Figure 1. The fuel-air measurements were conducted inside an experimental facility reminiscent of spherical combustion chambers with multiple access ports. The facility has a volume of 2 liters and has a rating of handling pressures up to 200 bar. The facility has been tested with temperatures of up to 600 K and is optically accessible. The facility is equipped with a Piezo Electric Pressure sensor, a K type thermocouple, a platinum four-prong spark plug, and an oxygen sensor. The fuel injector used in this experiment is a multipoint high-pressure fuel injector. The combustion event is captured by a high-speed camera (Photron Fastcam) and an image splitter, which is able to split the C2 * and CH* signals. The image splitter consists of an image doubler and a C_2*, and a CH* filter. The Fastcam captures these two signals, and then the C_2* signal is divided by the CH* and compared to the equivalence ratio of the exhaust gases[1-2]. Using this, the calibration curves of different biofuels fuel and their blends are generated, which are then used to gain a fuel-air distribution map of each biofuel.

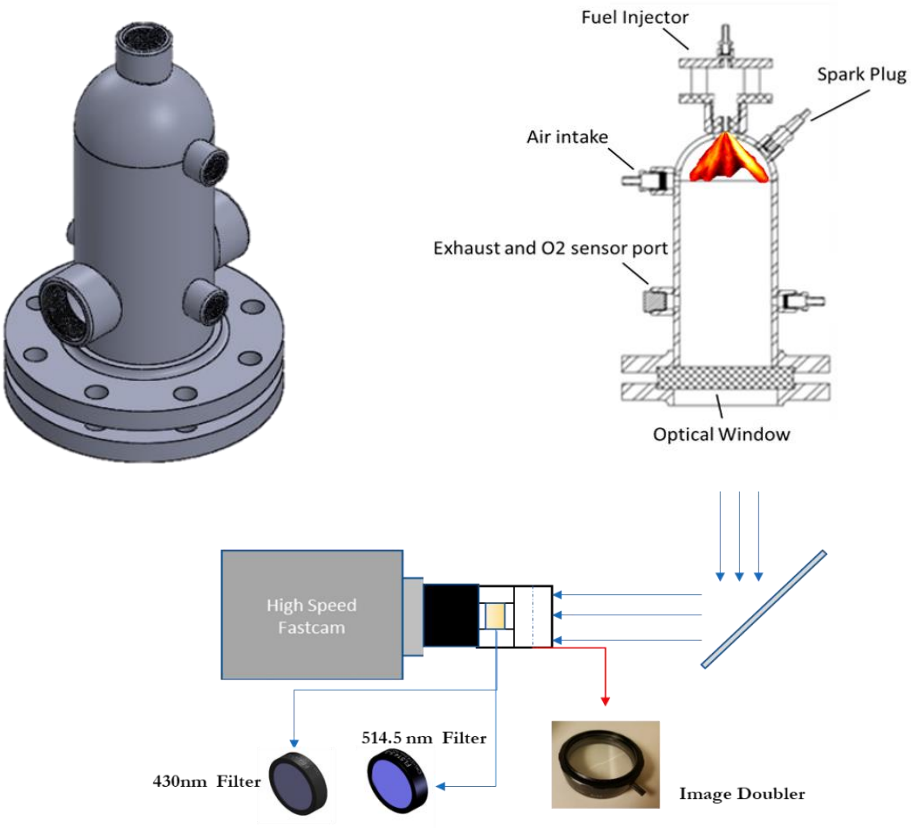

Figure 7: Experimental apparatus

The local C_2*/Ch* distribution that correlates to equivalence distribution is illustrated in figure 2. This figure is an intensity ratio map of neat diesel attained during combustion. It can be seen from this contour map that this map provides quantitative local information of the spatial distribution of fuel-air associated with an inhomogeneous/stratified combustion event. Also, this contour map also portrays the spatial region of interest studied for each biofuel blend. As shown in Figure 2, the spatial region of interest is studied for each of the flame tulips associated with each case. The region of interest location stays constant for every fuel blend studied. Within this ROI, 5 cross-sections are taken to study the equivalence ratio variability across the flame tulip; this procedure is repeated across all the flame tulips and averaged. The spatial variation of C_2* and Ch* intensity across the flame tulip is compared between the neat diesel and the other fuel blends to understand the variability of equivalence ratio across each fuel given by the calibration function. The combustion event is studied at 1.5 ms after ignition has occurred. Also, the intensity ratio has been normalized in order to compare with the baseline Diesel case.

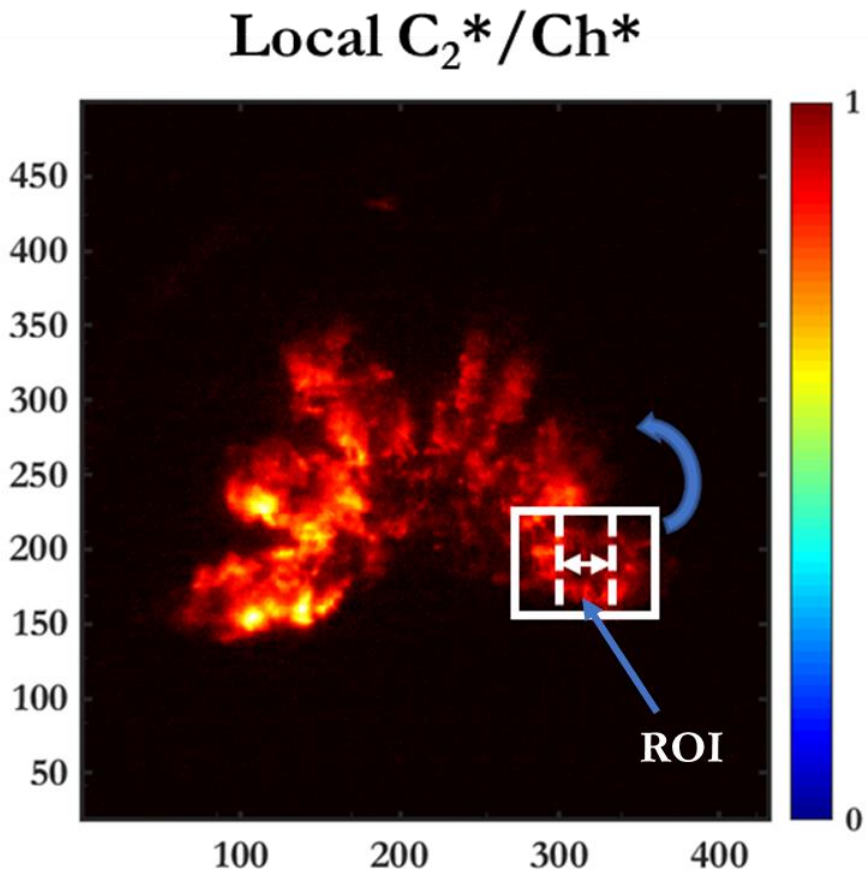

Figure 8:Normalized Intensity ratio map which is correlated to a calibrated equivalence ratio function.

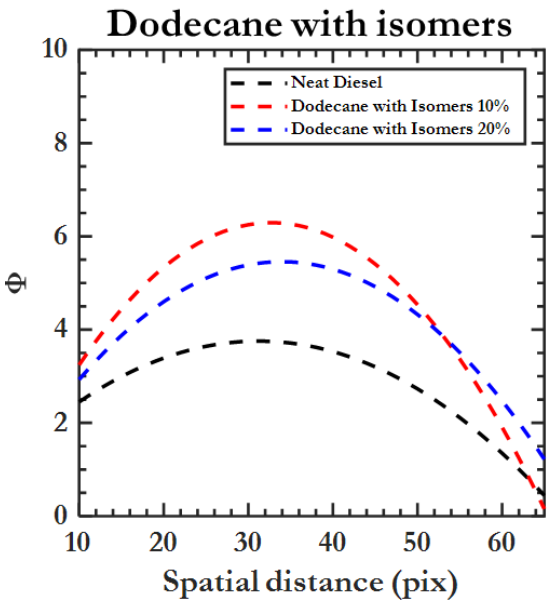

Figure 10: Local Φ distribution of Dodecane with Isomers across flame tulip cross section

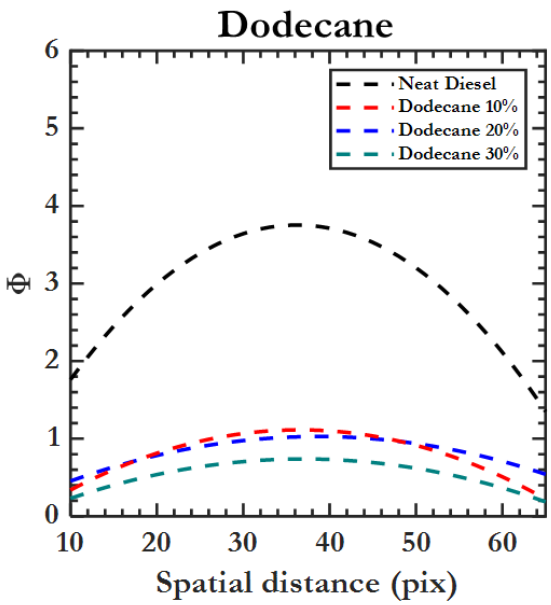

Figure 9: Local Φ distribution of Dodecane across flame tulip cross section

Based on the comparison between the volume blend percentage of Dodecane with Isomers with Neat Diesel, it is observed that the local equivalence ratio distribution across flame tulip associated to 10 and 20 percent blend is more than neat diesel. Figure 4 shows that the equivalence ratio value profile across the flame tulips for Dodecane is substantially less than diesel. This fuel also observed that as the blend percentage increased, the equivalence ratio value profile also increased. This behavioral trend is shared amongst all the blends; as the blend percentage increases from 10 to 30 percent, the equivalence ratio's local spatial distribution across the flame tulip decreases. From observing Figure 5, it is found that the equivalence ratio profiles for the Formaldehyde Dibutyl Acetyl blends are lower than the profile associated with diesel, and it can be further noticed that as the volume percentage of Formaldehyde Dibutyl Acetyl increases, the equivalence ratio profile associated with it decreases. This behavior is seen as stated before for all the blends. However, it is noticed that the 10 percent Nonanol blend equivalence profile is greater than the profile related to Formaldehyde Dibutyl Acetyl; however, for the 30 percent blend, the equivalence ratio value profile for Formaldehyde Dibutyl Acetyl is more than Nonanol. It is found that the local equivalence ratio distribution associated with 30 percent of Nonanol is less than all the blend studied in this experimentation. This behavior is seen between figures 8-10, which compares the local equivalence ratio distribution between each fuel and keeping the blend percentage constant. It is found from analyzing figures 8-10 that the equivalence ratio distribution

for the 10 percent blend is the least for Butylcyclohexane, and for both 20 and 30 percent, this behavior is found in Nonanol.

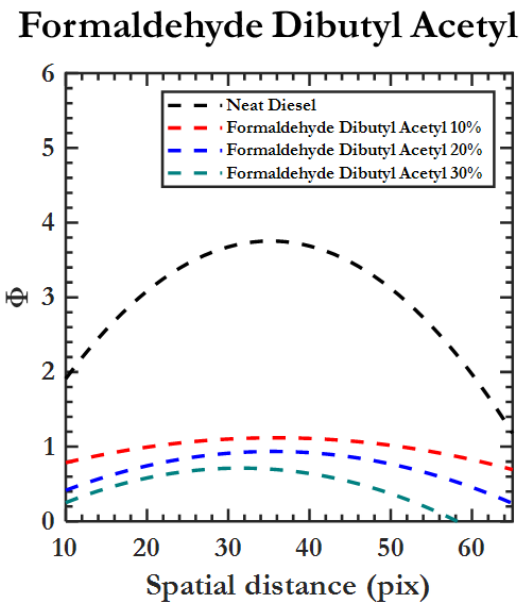

Figure 11: Local Φ distribution of Formaldehyde dibutyl Acetyl across flame tulip cross section

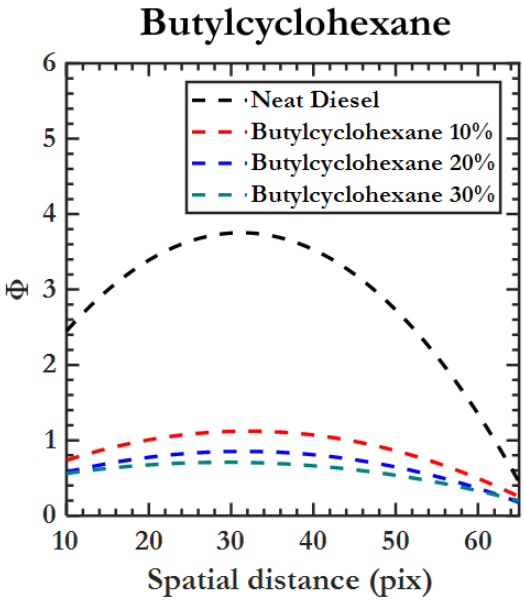

Figure 12:Local Φ distribution of Butylcyclohexane with Isomers across flame tulip cross section

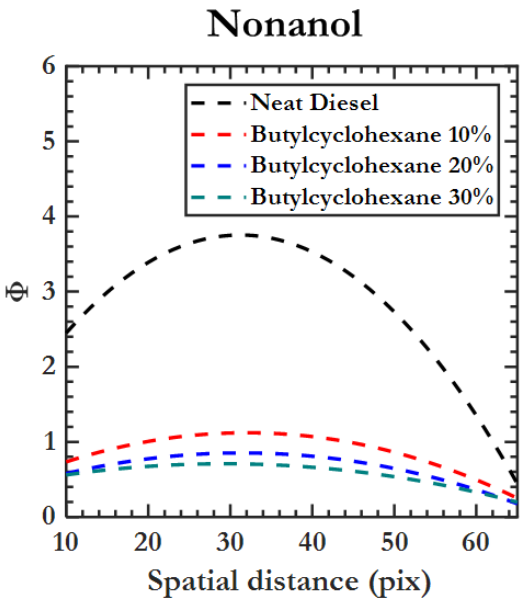

Figure 14: Local Φ distribution of Nonanol with Isomers across flame tulip cross section.

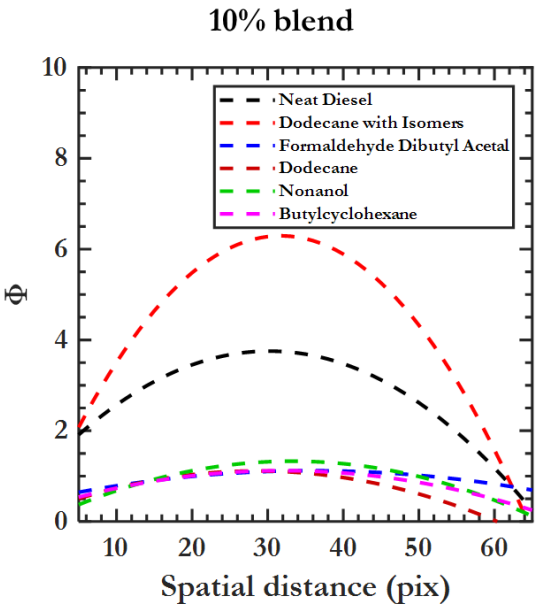

Figure 13: Local Φ distribution of 10 percent blends across flame tulip cross section

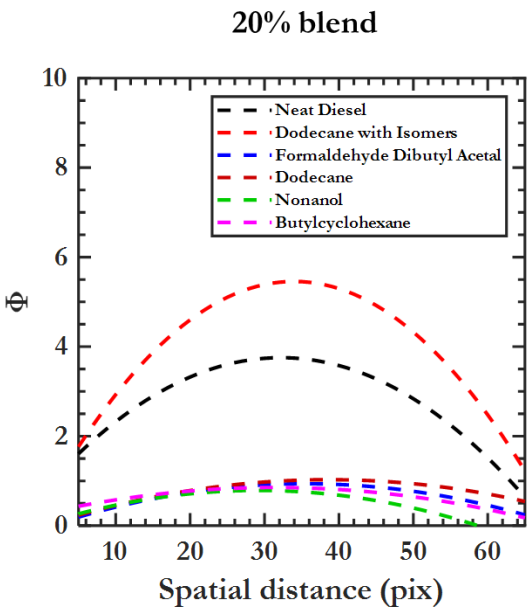

Figure 16: Local Φ distribution of 20 percent blends across flame tulip cross section

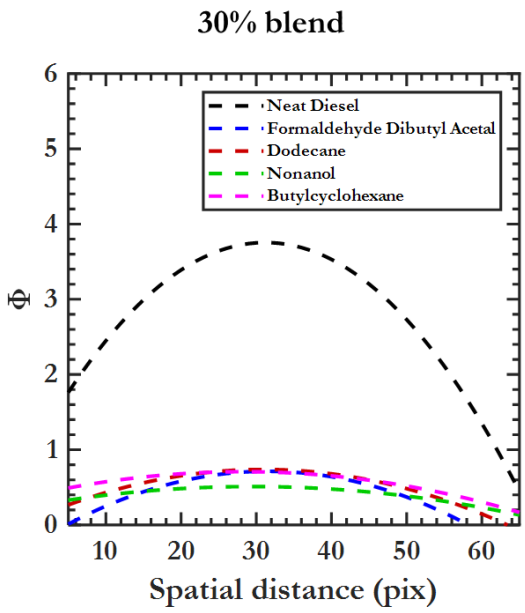

Figure 15: Local Φ distribution of 30 percent blends across flame tulip cross section

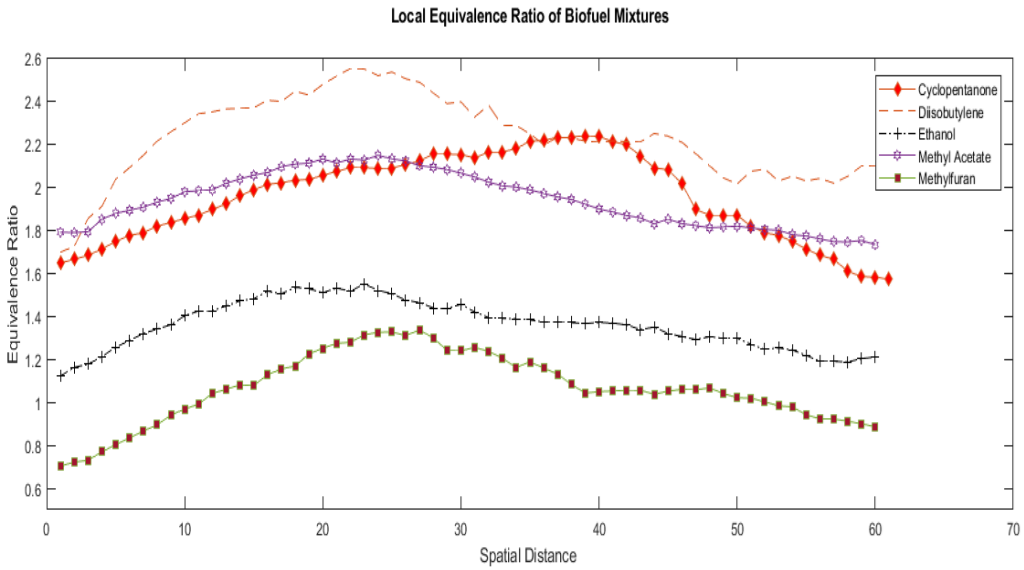

References:

[1] S. N. Soid and Z. A. Zainal, "Spray and combustion characterization for internal combustion engines using optical measuring techniques - A review," *Energy*, vol. 36, no. 2, pp. 724–741, 2011.

[2] E. H. Richards, G. A., Straub, D. L., and Robey, *Combustion Instabilities in Gas Turbine Engines: Operational Experience Fundamental Mechanisms, and Modeling*, vol. 1. .

[3] I. Ruiz-Rodriguez, R. Pos, T. Megaritis, and L. C. Ganippa, "Investigation of Spray Angle Measurement Techniques," *IEEE Access*, vol. 7, pp. 22276–22289, 2019.

[4] H. J. Kim, S. H. Park, and C. S. Lee, "A study on the macroscopic spray behavior and atomization characteristics of biodiesel and dimethyl ether sprays under increased ambient pressure," *Fuel Process. Technol.*, vol. 91, no. 3, pp. 354–363, 2010.

[5] J. V. Pastor, J. Arrégle, and J. M. García, and L. D. Zapata, ''Segmentation of diesel spray images with log-likelihood ratio test algorithm for non- Gaussian distributions,'' Appl. Opt., vol. 46, no. 6, pp. 888–899, 2007.

[6] J. Kang, C. Bae, and K. O. Lee, ''Initial development of non-evaporating diesel sprays in common-rail injection systems,'' Int. J. Engine Res., vol. 4, no. 4, pp. 283–298, Aug. 2003.

[7] R. Payri, F. J. Salvador, J. Gimeno, and J. de La Morena, ''Macroscopic behavior of diesel sprays in the near-nozzle field,'' SAE Int. J. Engines, vol. 1, no. 1, pp. 528–536, 2009

[8] L. M. Pickett, J. Manin, C. L. Genzale, D. L. Siebers, M. P. B. Musculus, and C. A. Idicheria, ''Relationship between diesel fuel spray vapor pen- etration/dispersion and local fuel mixture fraction,'' SAE Int. J. Engines, vol. 4, no. 1, pp. 764–799, 2011.

[9] S. H. Park, S. H. Yoon, and C. S. Lee, ''Effects of multiple-injection strategies on overall spray behavior, combustion, and emissions reduction characteristics of biodiesel fuel,'' Appl. Energy, vol. 88, no. 1, pp. 88–98, Jan. 2011.

Task 2.3 Laminar Flame Speed Measurements:

When considering a measurement from the laminar flame setup used in this work, it is necessary to consider the environment in which the phenomena occurs. Within Fig. 1 both a series of time progression images characteristic of a flame's evolution, corresponding to the red trace on the graph, are shown. From the flame progression several important things can be seen, at t_0, there are two electrode tips which form a spark gap where permitted after a piece of ceramic insulation; following the ignition spark, the early onset of a flame kernel can be seen. At t1, the flame has progressed radially outward having burned gasses within the central radii of the flame and unburned gasses outside; at this time, it is also permissible to verify the symmetry which forms for the corresponding laminar flame. At the later timestep t2, it is important to verify that there are negligible surface contours as these indicate non-laminar behavior; the shown surface contour is considered acceptable and is to be expected due to the asymmetry in the reaction environment imposed by the ceramic insulation.

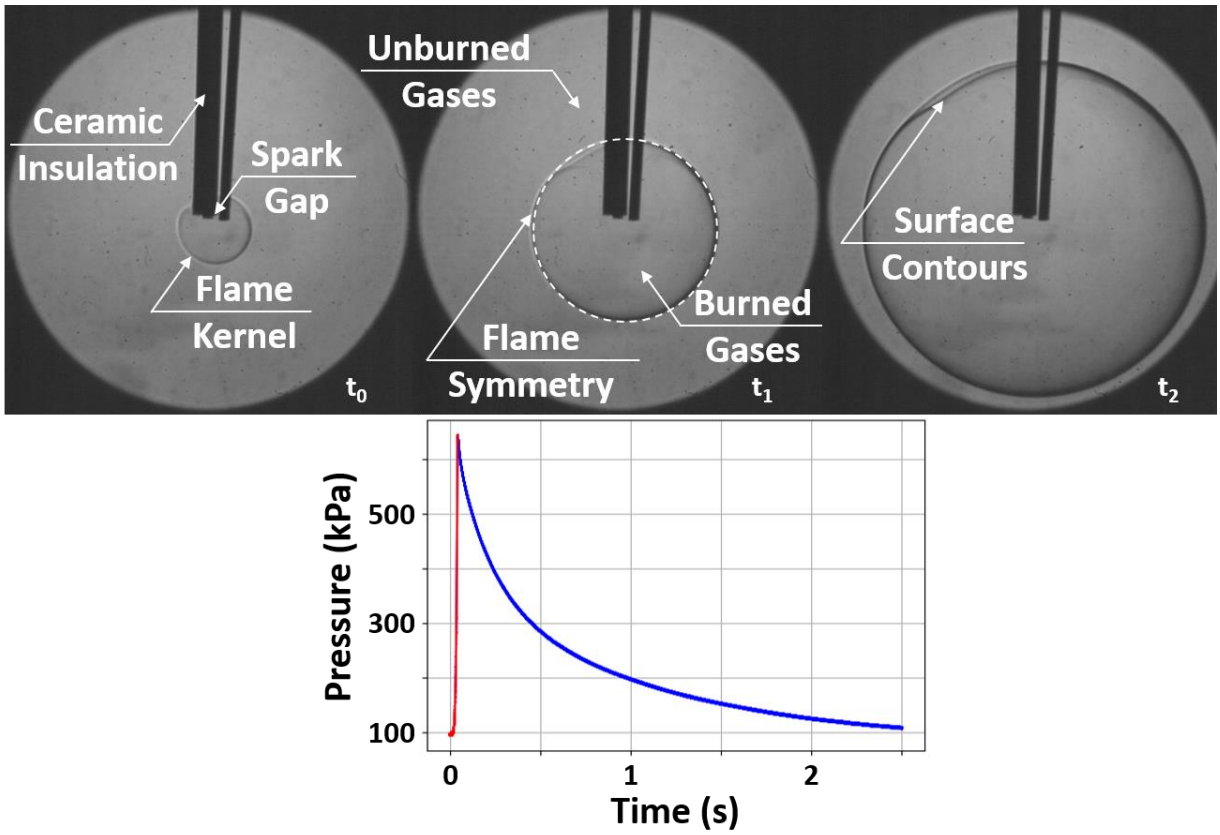

Fig. 1: Progression of a spherical laminar flame, and corresponding pressure trace. Rising is indicated in red, while falling is indicated in blue.

With the basics of the diagnostic method understood it is then permissible to understand the importance of the laminar burning velocity (LBV) as a measurement. Such LBV is the rate at which an unburned mixture travels perpendicular to a flame. LBV may be used as an indicator of: combustion efficiency, emissions output, and as a key metric for the evaluation of chemical reaction mechanisms. To obtain a finite number for LBV, it is necessary to impose restrictions on the combustion characteristics with the most important being the assumption of "constant volume" which is qualitative based on the pressure variability of the experiment. Subsequent assumptions derived from this constant volume depiction of the flame include: (i) negligible heat loss through the reaction vessel walls, (ii) isentropic compression of the flame, (iii) negligible influence of buoyancy and (iv) there is a thin smooth and uniform spherical flame with thickness on the order of microns.

To obtain flame speed measurements, a radial coordinate system is affixed to the center of the spherical flame, Fig. 2A. Which then enable the determination of LBV ($\boldsymbol{S_{u,L}}$) from eq. 1; for which the chamber radius ($\boldsymbol{R_o}$), initial pressure ($\boldsymbol{P_o}$), ratio of specific heats ($\boldsymbol{\gamma}$), flame radius ($\boldsymbol{r_f(t)}$) and pressure ($\boldsymbol{P(t)}$)at some point in time, and the determination of the rate of mass fraction of fuel consumed ($\frac{\boldsymbol{dX}}{\boldsymbol{dt}}$). Considerations of the rate of fuel rate of fuel consumption are quite complex, simple models have been used witch consider a single discrepancy layer at the flames surface (Fig. 2B) while a more accurate model discretizes, at each time step, concentric shells of the flame and reaction environment (Fig. 2C) in which a lumped parameter of

temperature and species concentration measurements are computed using software until there is convergence of the observed data and mass consumption.

$$S_{u,L} = \frac{{R_o}^3}{3 \cdot r_f(t)^2} \cdot \frac{P_o}{P(t)}^{1/\gamma} \cdot \frac{dX}{dt} \qquad \text{(eq. 1)}$$

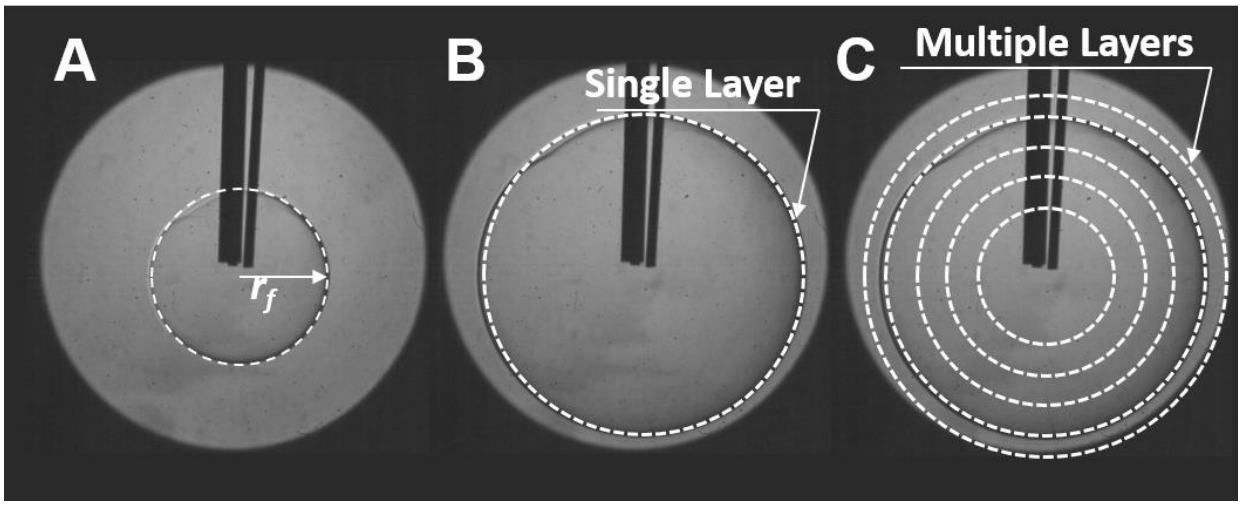

Fig. 2: (A) Definition of coordinate domain, (B & C) correspond with representation of a single and multi-layer model of temperature and composition.

Experimental Approach: Spherical Flames

The experimental apparatus used to obtain flame speed measurements is shown below in Fig. 3. Within this diagram there are several key components: (i) Filling equipment, (ii) reaction housing, (iii) diagnostic & ignition. Filling equipment (i) consists of a pair of High (100 – 10,000 torr) and Low (0.01-100) torr Baratrons; reagent supply tanks, a mixing tank, liquid fuel injection port, vacuum pump and exhaust. The reaction housing (ii) consists of a custom made spherical vessel with sapphire windows contained within a furnace for initial temperature control. (iii) Diagnostic's within this setup occur in two forms, the first consists of an LED emitter which projects a uniformly lit set of photons through the combustion chamber, which enables Schlieren image capture using a high speed camera; the second component of diagnostic equipment is derived from the dynamic Kistler pressure transducer which enables pressure measurements to be taken in excess of 1 MHz, though a high speed DAQ. Ignition is controlled on this device using a specially made ignition coil circuit triggered by a DAQ signal.

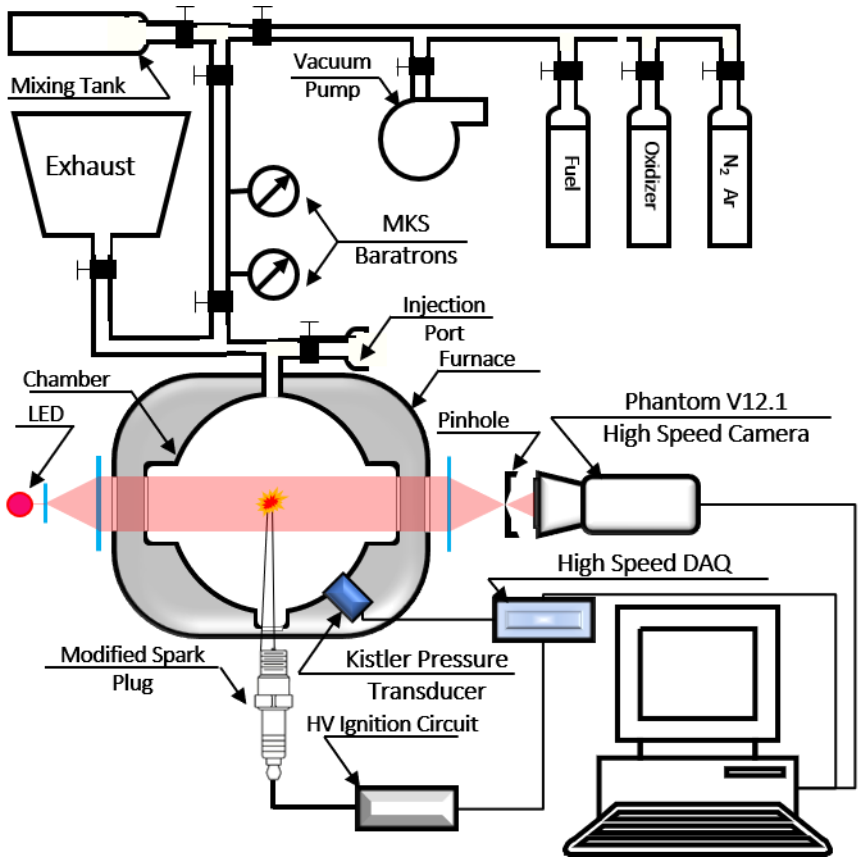

Fig. 3: Apparatus used for flame speed measurement obtainment.

Results and Discussion: Spherical Flames

Within Fig. 4, the obtained LBV for the selected fuels are shown. There is an expected uncertainty of ±2.5% in each of the obtained measurements. Over the range of equivalence ratios tested, velocities range between 0.25 and 0.90 m/s. Of interest are the LBV comparisons of 2-Methyl Furan, and cyclopentanone which closely coincide with those of ethanol and should be strongly considered for further study based on these findings as drop in ethanol replacements. It can be also seen that at higher equivalence ratios, there are similarity between the LBV of both methyl acetate and diisobutylene

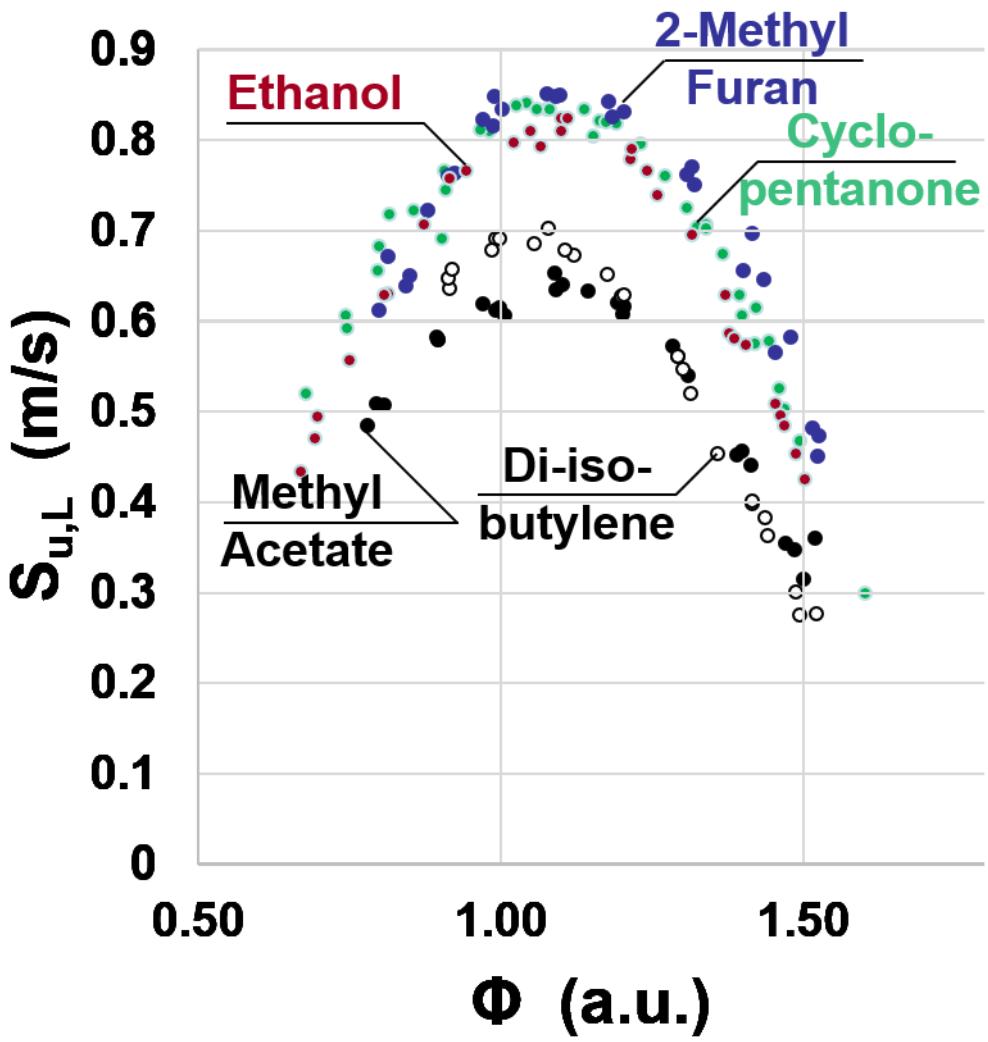

Fig. 4: Obtained laminar burning velocity measurements (±2.5%) for the selected fuels over a range of equivalence ratios and at initial temperature and pressure of 428±4 K and 1.00±0.02 atm.

Seven biofuels for drop-in gasoline replacements were selected for subsequent laminar burning velocity (LBV) measurements: (**i**) ethanol, (**ii**) cyclopentanone, (**iii**) methyl acetate, (**iv**) 2-methylfuran, (**v**) (α+β) diisobutylene, (**vi**) prenol, and (**vii**) isoprenol. Measurements were taken across a range of equivalence ratios. Of the evaluated fuels, laminar flame speeds of ethanol, cyclopentanone, and 2-methlyfuran were highest and similar in from equivalence ratio of 0.7 to 1.5. Methyl acetate flame speed is the lowest, with significant deviation below equivalence ratios of 1.1. Flame speeds of prenol and isoprenol, which can boost octane number were comparable to diisobutylene flame speed. Above equivalence ratios of 1.1, diisobutylene flame speed is similar to methyl acetate, prenol, and isoprenol.

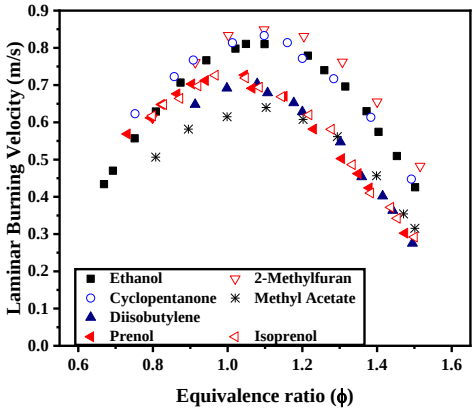

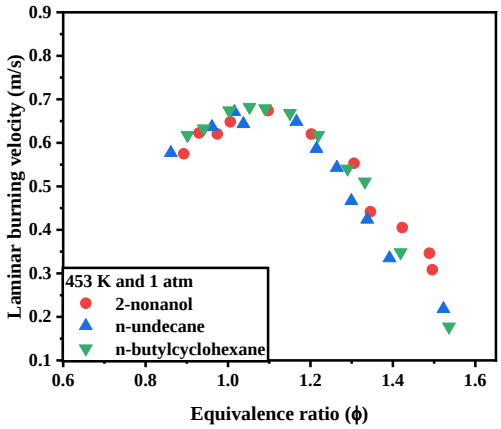

A similar set of experiments was conducted for three biodiesel alternatives: (**i**) 2-nonanol, (**ii**) n-undecane, and (**iii**) n-butylcyclohexane. These experiments were conducted in synthetic air at 453 K and 1 atm. Over the range of evaluated equivalence ratios, for lean conditions to equivalence of 1.2, all fuels showed similar burning velocities. However, at equivalence ratios above 1.2, there is a decay in the laminar burning rate of n-undecane and n-butylcyclohexane compared to 2-nonanol.

Publication:

[3] Zhang, K., Capriolo, G., Kim, G., Almansour, B., Terracciano, A. C., Vasu, S. S., Pitz, W. J., and Konnov, A. A. "**Experimental and Kinetic Modeling Study of Laminar Burning Velocities of Cyclopentanone and Its Binary Mixtures with Ethanol and n-Propanol**," *Energy & Fuels* Vol. 34, No. 9, 2020, pp. 11408-11416.

[2] Erik Ninnemann , Gihun Kim , Andrew Laich , Bader Almansour , Anthony C. Terracciano , Suhyeon Park , Kyle Thurmond , Sneha Neupane , Scott Wagnon , William J. Pitz , Subith S. Vasu; "**Co-optima fuels combustion: A comprehensive experimental investigation of prenol isomers**", Fuel 254 (2019): 115630

[1] Gihun Kim; B. Almansour; S. Park; A. C. Terracciano; K. Zhang; S. Wagnon; W. J. Pitz; Subith Vasu; "**Laminar burning velocities of high-performance fuels relevant to the Co-Optima initiative**", SAE International Journal of Advances and Current Practices in Mobility, 2019

Presentation:

[6] Gihun Kim, Anthony C. Terracciano, and Subith Vasu. "**Laminar burning velocity measurements of high-performance jet fuel/air mixtures**", AIAA Scitech 2020 Forum, (AIAA 2020-0639)

[5] Gihun Kim, Bader Almansour, Suhyeon Park, Anthony C. Terracciano, and Subith Vasu. "**Laminar Flame Speed Measurements of Alternative Liquid Fuels for Gas Turbines**", 2019 Clearwater Clean Energy Conference

[4] Gihun Kim, Bader Almansour, Suhyeon Park, Anthony Terracciano, Subith Vasu, Kuiwen Zhang, Scott Wagnon, William Ptiz, "**Laminar Burning Velocities of high-Performance Fuels Relevant to the Co-optima Initiative**," SAE Technical Paper 2019-01-0571,2019

[3] Gihun Kim, Suhyeon Park, Anthony C. Teracciano, Bader Almansour, Scott Wagnon, Bill Pitz, Subith Vasu, "**Laminar burning velocities of prenol – a "hyperboosting" fuel relevant to the Co-Optima initiative**", 11th U.S. National Combustion Meeting, Pasadena, CA, 3/2019, Paper no: 71LF-0201

[2] Gihun Kim, Bader Almansour, Anthony C. Terracciano, Suhyeon Park, and Subith Vasu. "**Laminar burning velocity measurements in methyl ester/air mixtures**", AIAA Scitech 2019 Forum, (AIAA 2019-0456)

[1] Gihun, Kim, Bader Almansour, Subith Vasu "**Premixed Flame Progagation in Mixtures of Cylopentanone/Air**" 2018 Estern States Section of the Combustion Institute, State College, PA, 2018

Task 2.4: Soot Volume Fraction and Induction Time Measurements

UCF's shock tube and laser based soot extinction measurements.

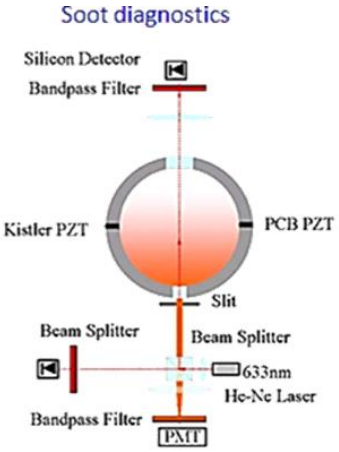

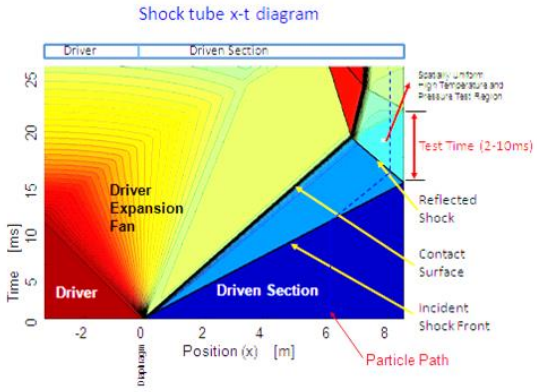

- **Baseline Mixture:**
  - **2.5% C_2H_4/0.75%O_2/96.75%Ar**
- **φ = 10.0**
- **1700 ≤ T ≤ 2200K, 4 ≤ P ≤ 5 atm**
- **Carbon fraction held constant at 5%.**
  - **C_2H_4 was reduced to 1.875% + blend fuel**
- **Fuels were added into the mixture and consisted of 25% of the total carbon.**
- **Soot extinction was measured using a HeNe laser at 632.8 nm.**
- **Soot Yield for all experiments were taken at 1.5ms = $\frac{[C]_{exp}}{[C]_{total}}$**

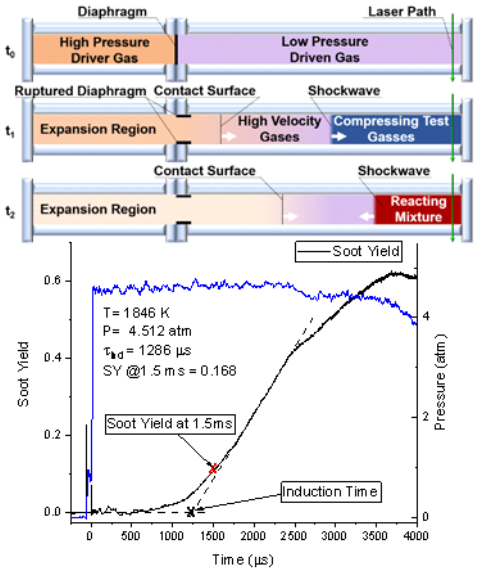

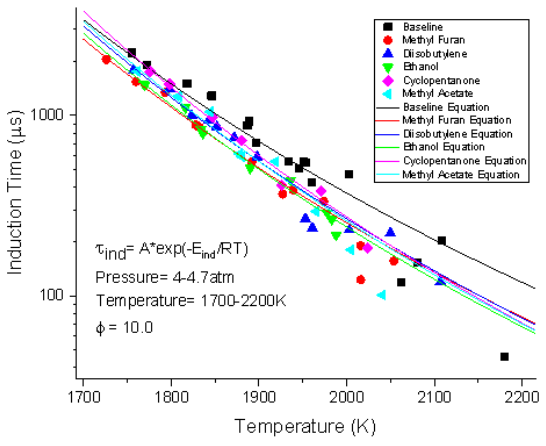

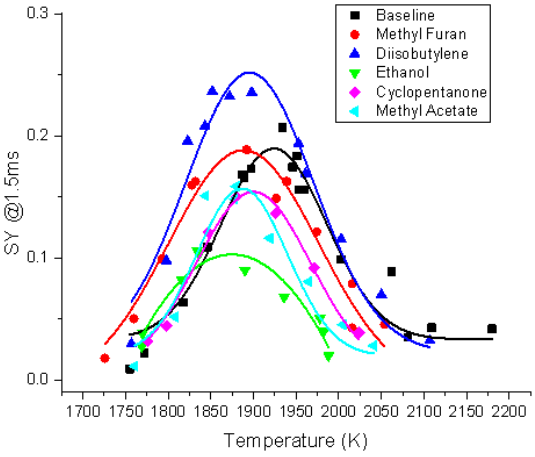

1. Fuels and composition.

Following table shows the biofuels received from NREL and their composition used in experiments.

Sr. No.	Name	Composition
1	n-butylcyclohexane	0.2% $C_{10}H_{20}$, 1.5% C_2H_4, 0.75% O_2, bal Ar.
2	n-undecane	0.18% $C_{11}H_{24}$, 1.5% C_2H_4, 0.76% O_2, bal Ar.
3	Farnesane	0.13% $C_{15}H32$, 1.5% C_2H_4, 0.86% O_2, bal Ar.
4	2-nonanol	0.22% $C_9H_{20}O$, 1.5% C_2H_4, 0.75% O_2, bal Ar.
5	Methyl decanoate	0.18% $C_{11}H_{22}O_2$, 1.5% C_2H_4, 0.83% O_2, bal Ar.

The composition of ethylene baseline mixture was 2.5% C_2H_4, 0.86% O_2 and balance argon. In all cases, carbon content was maintained constant at 5%.

2. Laser setup.

Laser-induced extinction method was used to measure soot volume fraction time-histories using Thorlabs HNL225R He-Ne laser at 632.8 nm. The transmitted He-Ne laser signal passing through the test mixture and two wedged sapphire windows was collected on Newport 2032 detector equipped with a 632.8 narrow band-pass filter (Thorlabs FL632.8-1).
Soot volume fraction is obtained from

$$f_v = \frac{ln\left(\frac{I_0}{I_t}\right)_{Soot} * \lambda}{6\pi * E(m) * L} \qquad 3$$

Where λ is the absorption wavelength (632.8 nm) and E(m) is the soot refractive index. E(m) is calculated to be 0.227 using the correlation given by Chang and Charalampopoulos[4]. The highest uncertainty associated with soot volume fraction measurements comes from the uncertainty in E(m) value. Assuming an uncertainty in E(m) of 50% as in[5], total uncertainty is estimated to be 52%.

3. Results.

Figure 1 shows the soot volume fraction time histories obtained for ethylene baseline and all biofuel blends.

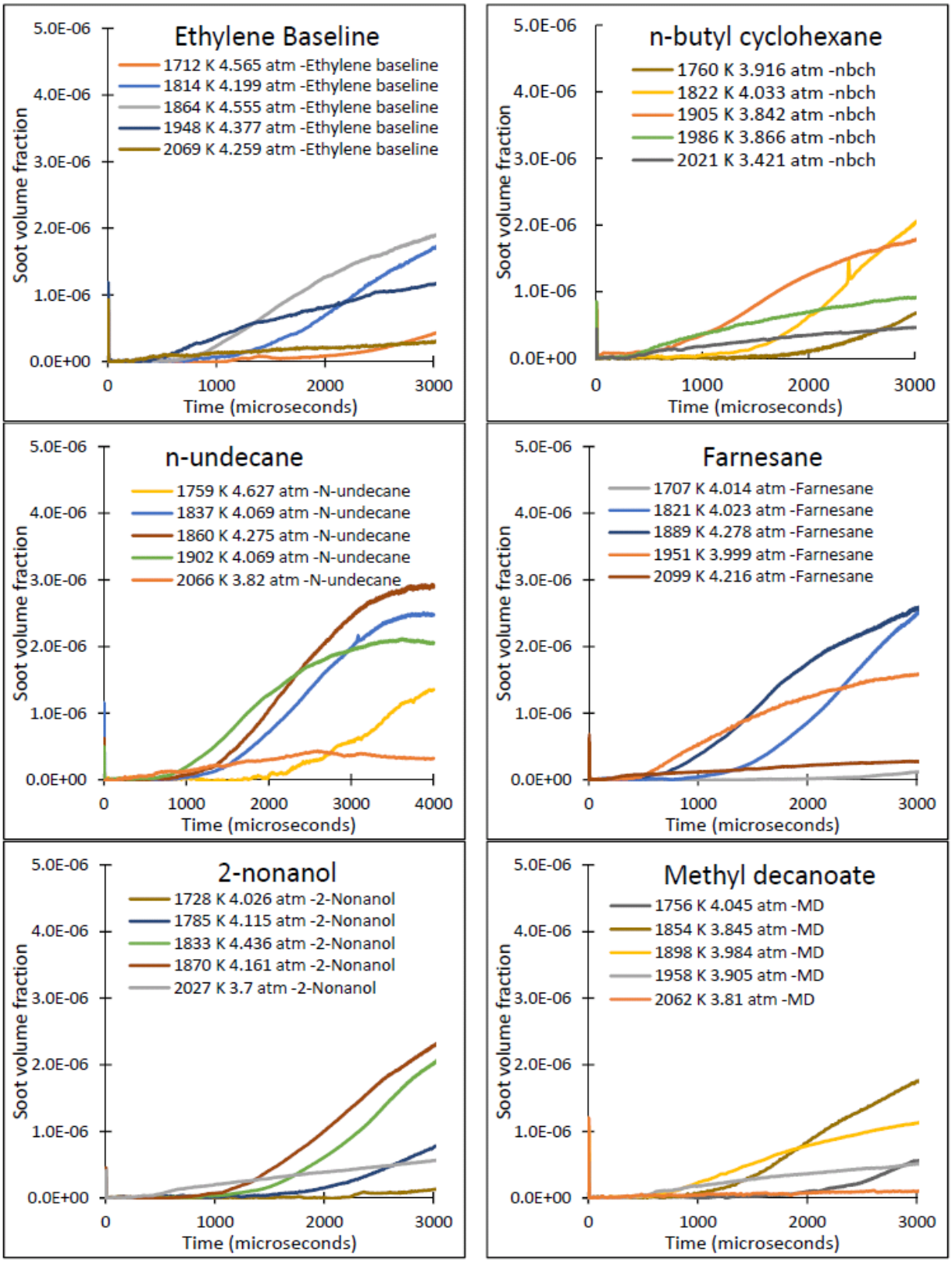

Figure 1. Soot volume fraction time-histories for oxidation of pure ethylene and different biofuel blends in ethylene.Induction time is the time when soot starts forming. In all cases, total carbon content in mixture is kept constant at 5%. For blends, 40% carbon is from biofuel and 60% from ethylene.

4. Conclusion.

Shock tube experiments were conducted to understand the sooting propensity of candidate fuels for blending/replacing diesel/jet fuel. The study was conducted from 1600 K to 2200 K and ~4 atm pressure. The data obtained in this work will be utilized to improve kinetic mechanism for all individual biofuels. This work completes the milestone for soot measurements subtask.

Task 2.5: Synchrotron Coupled Fundamental Autoignition Experiments

Oxidation reactions of neat α and β diisobutylene were conducted in a Jet Stirred reactor at conditions which replicated shortly after ignition. Reaction intermediates were sampled and analyzed using synchrotron photoionization mass spectrometry to identify key differences in the reaction processes for the fuel isomers. As this relatively short residence time is just after ignition, this study is targeted at the fuels' ignition events; in total, there was a direct identification of 25 oxygenated intermediates and 21 non-oxygenated intermediates. Ignition characteristics for both isomers were found to be strongly dependent on the kinetics of C_4 and C_7 fragment production and decomposition, with the tert-butyl radical as a key intermediate species. However, the ignition of α-DIB exhibited larger concentrations of C_4 compounds over C_7, while the reverse was true for β-DIB. These identified species will allow for enhanced engineering modeling of fuel blending and engine design.

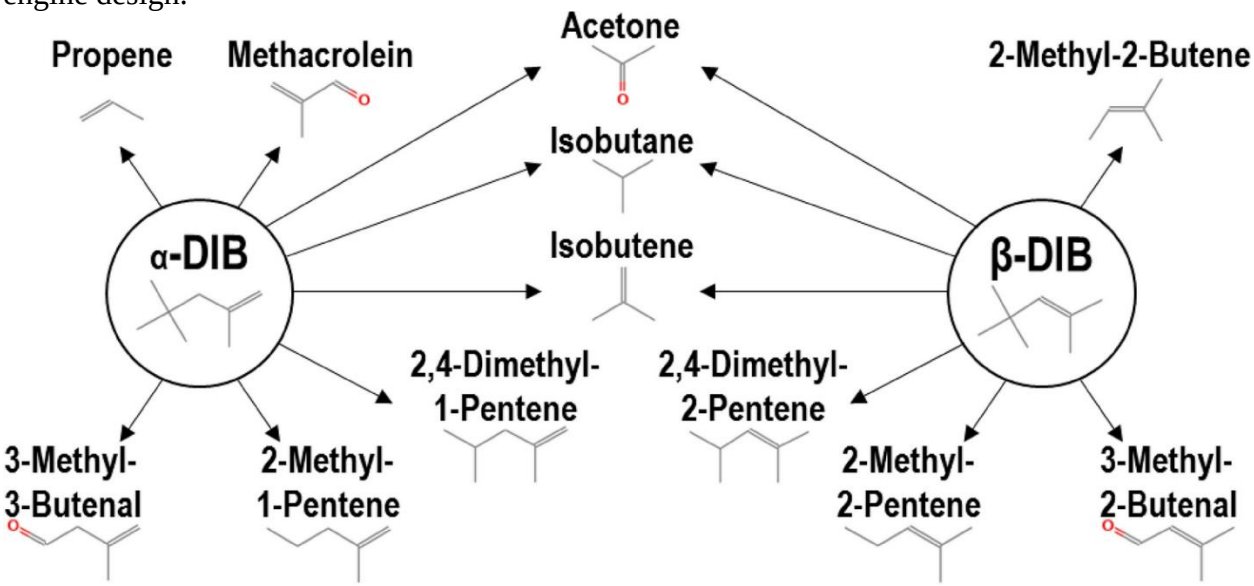

Publication:

[1] Terracciano, Anthony Carmine, et al. "**Elucidating the differences in oxidation of high-performance α-and β-diisobutylene biofuels via Synchrotron photoionization mass spectrometry.**" *Scientific reports* 10.1 (2020): 1-16.

ALS at Berkeley Natl Lab used for synchrotron photoionization studies

Dilution used to control residence time τ

Externally heated to lowest ignition temperature

- DIB 2 Ignites 70K lower
  - C=C bond location is assumed dictating behavior
- Formation of Formaldehyde in both tests
- Radicals heavier than the fuel species
- DIB1 more intermediate species <45 amu at T_{ig}
- DIB2 produces similar ratios of species at 55 amu in lower quantities

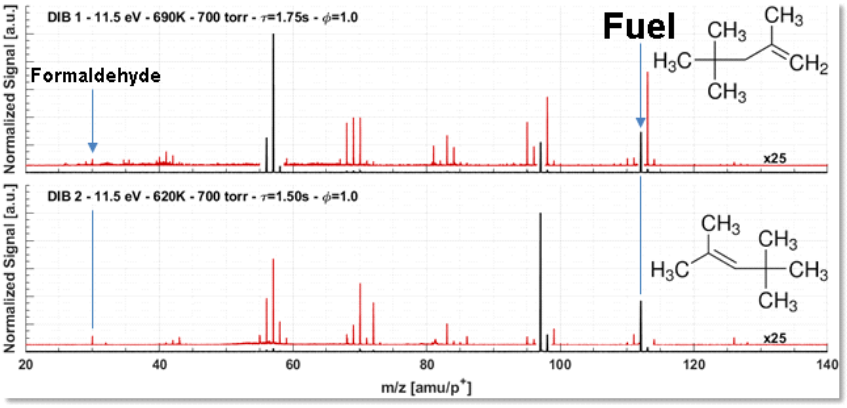

Task 2.6 Cylinder Carbon Deposit

Introduction

Soot formation from the incomplete combustion of hydrocarbons is a complex phenomena in which heated metal surfaces, local fuel-oxidizer mixtures, and other characteristics dramatically impact the formation of soot [4, 5]. Even in combustion which is assumed to be clean burning, polycyclic aromatic hydrocarbons (PAHs) are present in low concentration [6]. Experimental studies have shown that for a given set of engine operating criterion, the characteristics of the fuel injection pulse have a strong influence on the rate of production of soot versus NO_x species [7]. Additionally, the nominal carbon coordination structure of soot may be identified using Raman spectroscopy [8].

As it is known that different fuels will have unique sooting tendencies for all other engine criterion fixed, it is important to study soot formation [9]. As part of this Co-Optima study, a test rig has been devised which enables the collection of formed soot, from a fuel sprayed from a pulsed injector onto a heated sample coupon in a fixed environment. Following a fixed spray criterion, the sample coupon is then analyzed using Raman Spectroscopy in order to characterize the structure of the soot.

Experimental Approach

The experimental test rig to study soot formation from each investigated fuel is shown in Figure 4. Sample coupons of 18-8 stainless steel of 25.35±0.05 mm diameter, and mass of 3477.018±128 mg is placed on a heated coupon holder. Coupons were heated to 350 ˚C under an argon flow of 1 scfh and held for 10 minutes at 174.31±2 kPa and kept under a constant flow of argon for the duration of the experiment. The effluent gas is run through a water trap after exiting the test chamber. . Fuel is pumped into the injector using a pressurized Argon feed line held at a stagnation pressure of 174.31±2 kPa. Fuel was sprayed from a Bosch EV14 (PN 0 280 158 038) valve driven by a 12v pulse circuit. 200 fuel pulses, of 10 ms, were impinged onto the hot surface. Excess fuel which either fails to pyrolyze or vaporizes is allowed to condense and

collect in the fuel recovery reservoir or is carried off as vapor and run through the water trap. After pulsing the system was cooled to room temperature under flowing argon, disassembled and the coupon recovered for weighing to the nearest μg and Raman analysis.

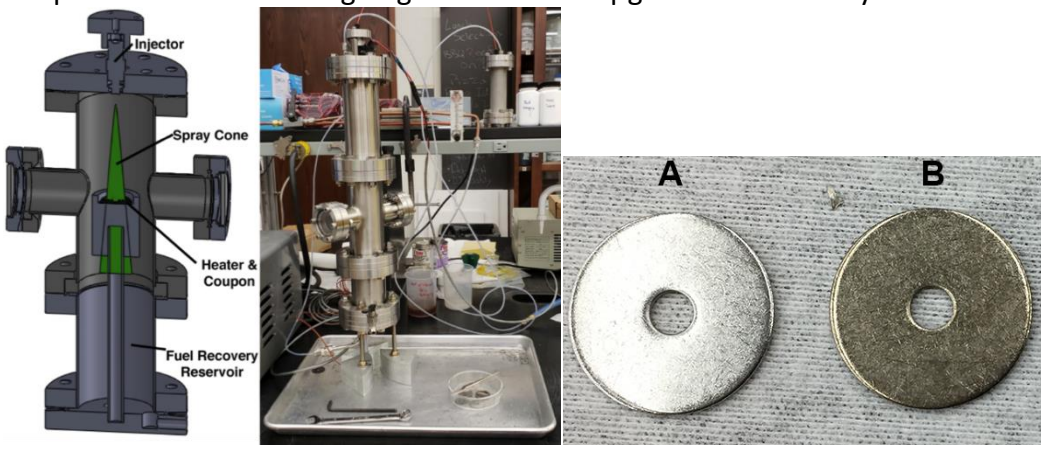

Figure 4: Soot formation test rig and Test coupons of 18-8 stainless steel held at temperature in the rig without hydrocarbon impingement (A) and with hydrocarbon impingement (B). The coupon on the right was exposed to 200 pulses of methyl acetate while at 350 ˚C.

After each run of the test rig, the sample coupon is removed, and the Raman Spectra of the carbon coating is analyzed using a Witec Alpha 300 confocal Raman spectrometer. For this analysis, a 532 nm excitation source is used with a grating having 1800 groves/mm enabling a minimum channel collection width of 0.9 cm^{-1}/pixel and a 50x objective lens. Scans are collected 10 times to acquire an averaged signal with sufficient signal to noise ratios. This process was repeated 5x per coupon Known peaks pertaining to carbon are then investigated.

Results & Discussion

Within Figure 5, the Raman Spectra for carbon deposition on an 18-8 stainless steel washer is presented along with that of n-dodecane spray. At the test temperature hydrocarbons undergo aromatization on hot metal surfaces produces graphitic carbon deposits. Although optically discernable, mass measurements were inconclusive. Raman spectral measurements were utilized to measure the level of surface graphitic carbon formation. At approximately 1300 and 1600 cm^{-1}, the *G* and *D* bands pertaining to carbon can be seen [10], which correspond to the relative ratios of sp^2 and sp^3 configurations of deposited soot [11]. It can be assumed these peaks indicate ordering, where a higher ratio of *D* to *G* indicates larger graphitic layers. Additional data presented in Tables 2.and 3.

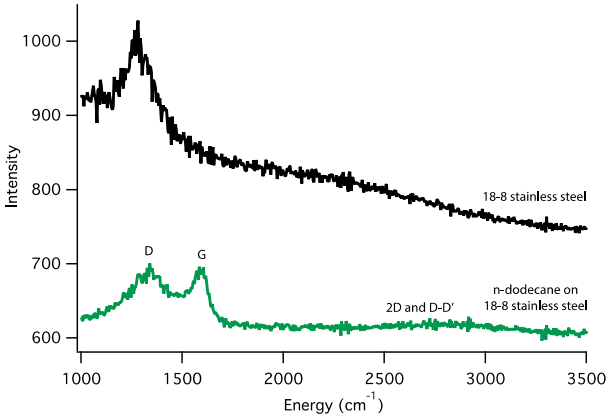

Figure 5. The Raman spectra of a pristine coupon (top) and one at 350 ˚C exposed to 200 pulses of n-dodecane shows the formation of graphitic carbon.

Table 1: Raman spectral data for carbon deposits formed on 18-8 stainless steel test coupons.

Compound	Energy (cm-1)	FWHM	D/G ratio	Size (µm)
Blank	1287.96 ± 0.17%	161.7 ± 4.2%	NA	NA
methyl acetate	1311.7 ± 0.29%	237.5 ± 3.6%	2.23 ± 6.1%	5.19 ± 6.2%
	1574.19 ± 0.18%	123.9 ± 9.7%		
2-methylfuran	1381.79 ± 0.16%	313.5 ± 2.4%	0.79 ± 2.6%	1.78 ± 2.7%
	1593.55 ± 0.01%	93.9 ± 2.1%		
cyclopentanone	1387.72 ± 0.33%	155.4 ± 9.5%	1.02 ± 5.7%	2.33 ± 5.8%
	1591.04 ± 0%	87.8 ± 2.9%		
diisobutylene	1368.74 ± 0.2%	355.4 ± 4.6%	1.1 ± 9.7%	2.52 ± 9.9%
	1591.86 ± 0.04%	95.8 ± 2.4%		
ethanol	1369.22 ± 0.14%	317.8 ± 1.3%	0.97 ± 8.3%	2.22 ± 8.6%
	1591.86 ± 0.02%	104.1 ± 1.6%		

Table 2: Raman spectral data for carbon deposits formed on 18-8 stainless steel test coupons.

Compound	Energy (cm-1)	FWHM	D/G ratio	Size (µm)
Dibutoxymethane	1373 ± 2%	305 ± 305%	1.04 ± 20.49%	2.09 ± 9.93%
	1592 ± 1%	133 ± 133%		
Butylcyclohexane	1391 ± 1%	355 ± 10%	1.04 ± 5.72%	2.39 ± 3.07%
	1579 ± 4%	111 ± 5%		
n-Dodecane	1358 ± 0%	278 ± 7%	0.93 ± 4.51%	2.12 ± 1.49%
	1589 ± 1%	98 ± 12%		
Dodecane isomers	1371 ± 2%	304 ± 25%	0.93 ± 14.90%	2.13 ± 12.22%
	1587 ± 0%	101 ± 21%		
1-nonanol	1357 ± 1%	277 ± 3%	0.93 ± 6.80%	2.12 ± 3.84%
	1588 ± 2%	95 ± 6%		

Table 3: Raman spectral data for carbon deposits formed on nickel test coupons.				
Compound	**Energy (cm-1)**	**FWHM**	**D/G ratio**	**Size (µm)**
Dibutoxymethane	1366 ± 1%	252 ± 21%	0.92 ± 12.73%	2.09 ± 9.93%
	1592 ± 1%	171 ± 20%		
Butylcyclohexane	1381 ± 3%	302 ± 27%	0.89 ± 6.94%	2.04 ± 3.88%
	1581 ± 2%	157 ± 36%		
n-Dodecane	1365 ± 1%	304 ± 14%	0.83 ± 0.92%	1.89 ± 0.92%
	1606 ± 1%	211 ± 16%		
Dodecane isomers	1367 ± 1%	236 ± 33%	0.84 ± 3.91%	1.92 ± 0.54%
	1585 ± 1%	151 ± 26%		
1-nonanol	1374 ± 1%	308 ± 44%	0.97 ± 3.57%	2.21 ± 0.64%
	1601 ± 2%	227 ± 57%		

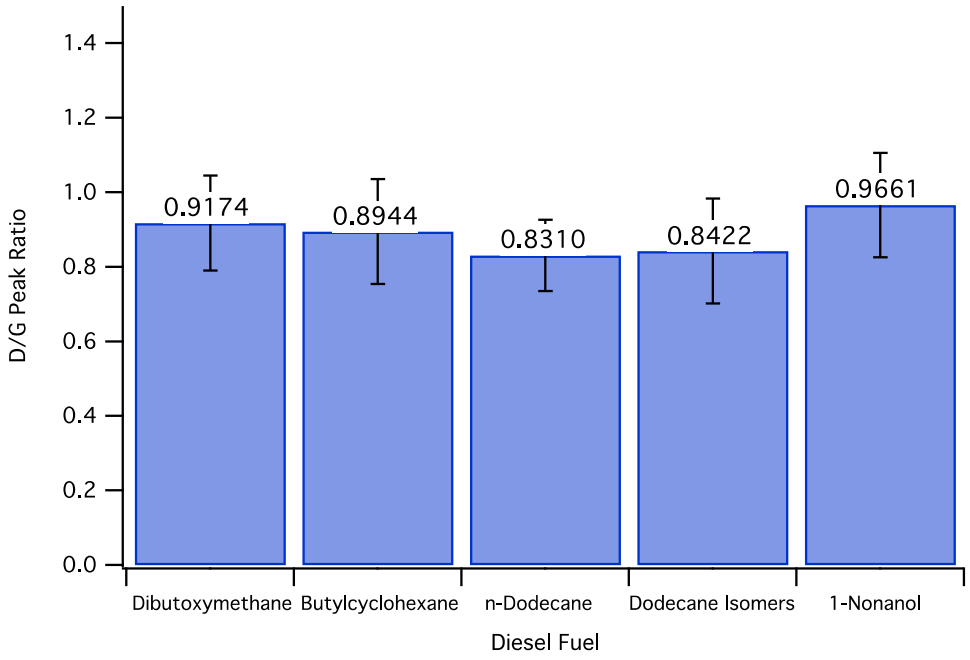

Figure 6. D/G ratios for fuels on pure nickel.

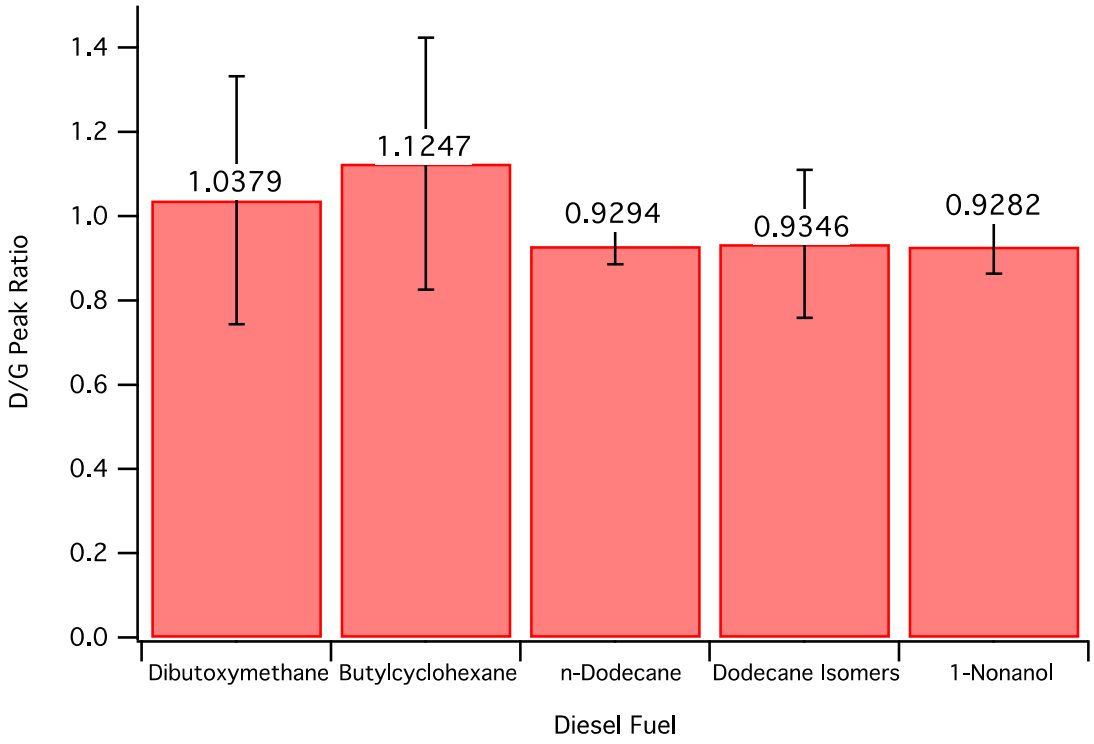

Figure 7. D/G ratios for fuels on 18-8 stainless steel.

Task 2.7: Fuel Volatility Measurements

Introduction

The volatility of fuel has measureable effects on engine performance. Fuels with high volatility will form vapor at lower temperatures relative to those with lower volatility. Low volatility fuels require hotter overall engine temperatures, which are ideal for diesel engine operation. Vapor pressure and distillation measurements are typically performed for fuel mixtures and similar measurements are not as constructive for analysis of pure compounds. As part of this study, we have determined a convienient procedure for measuring isothermal evaporation rates of our pure diesel analog compounds using thermogravimetric analysis, which ensures each sample is held at temperature with high accuracy and precision.

Figure 17. *Thermogravimetric analyzer measures mass of material in a small hanging pan while heating. Each fuel was pipetted onto a pan and the chamber held at 60°C until fully evaporated.*

Experimental Approach

Thermogravimetric analysis (TGA) was used in order to assess fuel volatility. Using a micropipette, 30 μL of each fuel was placed onto the alumina pan. The liquid sample was heated at a rate of 5°C/min to 60°C and then was held isothermal at 60°C until the entire sample evaporated.

Results and Discussion

Evaporation rates were very linear with the candidate compounds showing clear differences in evaporation rates (Figure 7). Values for evaporation rates were determined by plotting mass of fuel over time (graph not shown) and the slope of the curves calculated using plotting software. The values obtained are presented in Table 2. It is interesting to note that boiling point (vapor pressure) alone is not enough to describe the vaporization rate of the compounds. For example, 1-nonanol and dodecanes have similar boiling points but nearly an order of magnitude difference in vaporization rates. This result suggests that intermolecular interactions due to molecular functionality greatly affect fuel volatility.

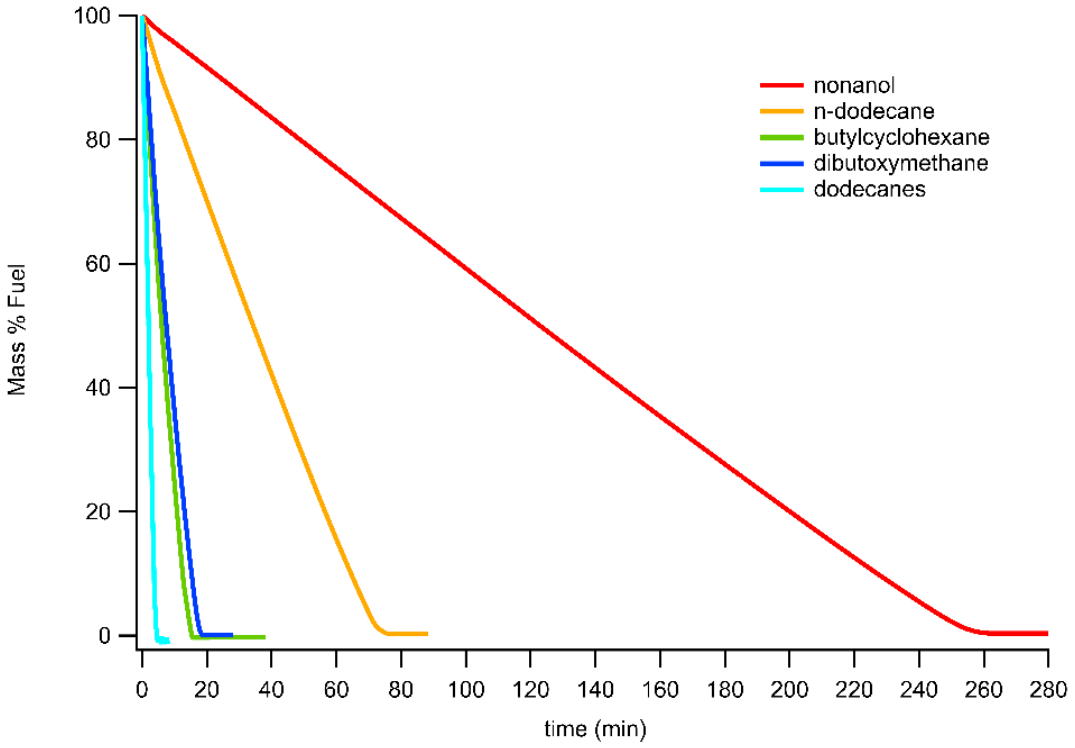

Figure 18. *Thermogravimetric analysis (TGA) showed that 1-nonanol had the slowest rate of evaporation while dodecane isomers had the highest rate of evaporation.*

Table 2. Evaporation rates of each diesel analog compound were calculated from the slope of a linear fit to each curve.

Diesel Compounds	**Evaporation rate (mg/min)**	**Linear fit**	**BP °C**
butylcyclohexane	0.3068 ± 0.000145	0.9996	178 - 180
dibutoxymethane	1.2763 ± 0.00518	0.9948	180
1-nonanol	0.10594 ± 2.71e-05	0.9999	215
n-dodecane	1.2098 ± 0.0039	0.9959	216.3
dodecanes	2.6708 ± 0.00459	0.9997	215 - 217

ASTM methods for fractional distillation of fuels. By fractionating the fuels we will thoroughly understand the volatility of a give fuel. In addition, each fraction will be analyzed by gas-chromatograph mass-spec (GC-MS) to correlate it chemical composition to the volatility data.

- Synthetic 96 RON was prepared from 56.7 v% isooctane, 33.3 v% toluene and 10.0 v% n-heptane.
- A boiling point reference blend was prepared by from 90 v% synthetic 96 RON and 10 v% pentane.
- Multiple samples were prepared of each fuel at 10 v% and 20 v%.
- Gas chromatography with mass sensitive detection (GC-MS) was performed with a Restek Rtx-1 capillary column
  - Rention time has excellent reproducibility
- Simulated distillation curves will be generated using Envantage's Dragon SimDist software.

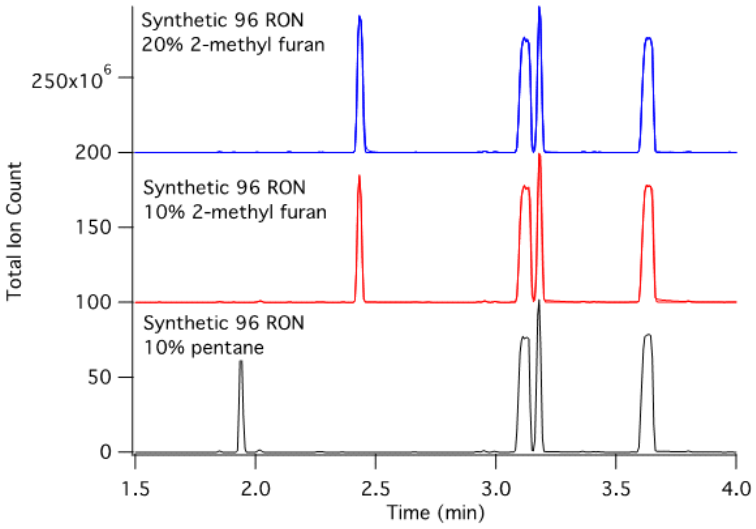

	Fraction (v%)	Boiling Point (°C)	Retention Time (min)	RT % Deviation	Peak Area	Peak Area %Deviation
96RON						
Iso-Octane	56.7	98	3.126	0.222	2118819548	3.616
Heptane	10.0	98.4	3.185	0.018	1125789366	0.508
Toluene	33.3	111	3.638	0.104	2055328973	5.346
10% Ethanol in 96RON						
Ethanol	10	78	1.748	0.033	418374721	3.891
Iso-Octane	51.0	98	3.122	0.018	1930891701	1.416
Heptane	9.0	98.4	3.185	0.018	988799067	1.142
Toluene	30.0	111	3.638	0.088	1962650396	0.927
20% Diisobutylene in 96RON						
Iso-Octane	45.3	98	3.125	0.074	1931063068	0.849
Heptane	8	98.4	3.183	0.000	990240591	0.916
2,4,4-trimethyl-1-pentene	7.5	101	3.279	0.000	1404288224	1.817
2,4,4-trimethyl-2-pentene	2.5	104	3.387	0.017	701996141	2.272
Toluene	26.7	111	3.632	0.000	1956459150	0.631
20% Methyl Acetate in 96RON						
Methyl Acetate	20.0	57.4	2.007	0.050	676773155	8.019
Iso-Octane	45.3	98	3.127	0.222	2108058936	2.581
Heptane	8.0	98.4	3.188	0.018	1106700718	1.789
Toluene	26.7	111	3.643	0.135	2135809896	2.708
20% 2-Methylfuran in 96RON						
2-Methylfuran	20.0	64	2.437	0.024	1376797714	4.006
Iso-Octane	45.3	98	3.121	0.000	2147821796	1.028
Heptane	8.0	98.4	3.184	0.018	1127875672	1.267
Toluene	26.7	111	3.633	0.000	2157700791	0.186

References

1. Quintero, S. A.; Schmitt, J.; Blair, R.; Kapat, J., Alternative Microturbine Fuels Feasibility Study Through Thermal Stability, Material Compatibility, and Engine Testing. *Journal of Engineering for Gas Turbines and Power* **2013,** *135* (11), 111401-111401. http://dx.doi.org/10.1115/1.4025128DOI: https://doi.org/10.1115/1.4025128

Task 2.8 Viscosity Measurements

Introduction

Fuel viscosity is an important engineering design parameter. Such information is necessary for adequate sizing of pumps for processing, transportation, and manufacturing of fuels as well as for key parameters of engine design. Quartz crystal microbalances (QCMs) have shown to be a unique tool for rapid and accurate determination of viscosity by measuring the change in the crystal's oscillating frequency in air and when submerged in a test liquid. In this study, a QCM is placed into a fuel bath blend of known temperature and composition. The change in oscillation frequency of the crystal after submersion is used to calculate the viscosity of the fuel or fuel blend in question. The viscosity fixture is equipped for the simultaneous measurement of density by suspending the fixture over a mass balance and measuring the change in mass of an invar standard. The ability to measure density of the fuel allows a more accurate calculation of viscosity.

Experimental Approach

A simple test fixture for the measurement of viscosity is shown in Figure 6(A). The density calculations are found using (eq. 3) which compares the apparent weight of invar in air and submerged divided by the volume of the sample.

$$\boldsymbol{\rho_L = \frac{W_{inv,air} - W_{inv,submerged}}{V_{invar}}} \qquad \text{(eq. 3)}$$

The figure illustrates the initial design in which the QCM can be raised and lowered into the fuel reservoir. . The QCM is coated with a non-reactive material: platinum (Pt); leads for the crystal which are exposed to the fluid are steel, which does not react with the organic solvents in question. This setup was soon upgraded to allow for a temperature-controlled bath and density measuring capabilities (Figure 6(B)). In the upgraded design, a jacketed beaker is implemented to control the bath temperature. The beaker is suspended above a balance but does not come in contact with the balancing pan. Around the beaker is a scaffolding which holds the hanging invar standard as well as the QCM. The scaffolding and QCM mass are known, as well as the mass of the invar standard in air. During the experiment, the QCM is placed within the empty beaker and 20 frequency measurements are taken in air. Following this, fuel is added to the beaker and the invar standard and QCM are submerged so that they entirely rest inside the evaluation fluid. The fuel, QCM, and invar standard are left to equilibrate with the bath temperature and stabilize. Measurements do not proceed until the fluctuations in fuel temperature during stabilization are less than ±0.1 °C, over a two minute period. This criterion must be satisfied for 8 minutes before 20 measurements of frequency and invar mass are taken for the submerged case. This

temperature stabilization further eliminates the effect of any equilibrium transition between the free ***oscillation frequency of the crystal in air (f_o)*** and the ***equilibrium oscillation frequency after being submerged in the fuel bath f_{act}*** which is used to calculated the ***frequency differential Δf*** (eq. 4). As the displacement of the crystal during oscillation is on the order of 1~10 μm and the Fuel Reservoir has a diameter of 101.6 mm, it can be ensured that there is no reflected wave interfering with the crystal's resonance. During the test, the liquid fuel is held at a fixed temperature of 25±0.05 °C, and is open to the ambient environment. To calculate ***viscosity*** η (eq. 5) is used where ***k is the calibration constant***.

$$\Delta f = f_o - f_{act} \quad \text{(eq. 4)}$$

$$\eta(\Delta f, \rho_L) = \frac{\Delta f^2}{k} \Big/ \rho_L \quad \text{(eq. 5)}$$

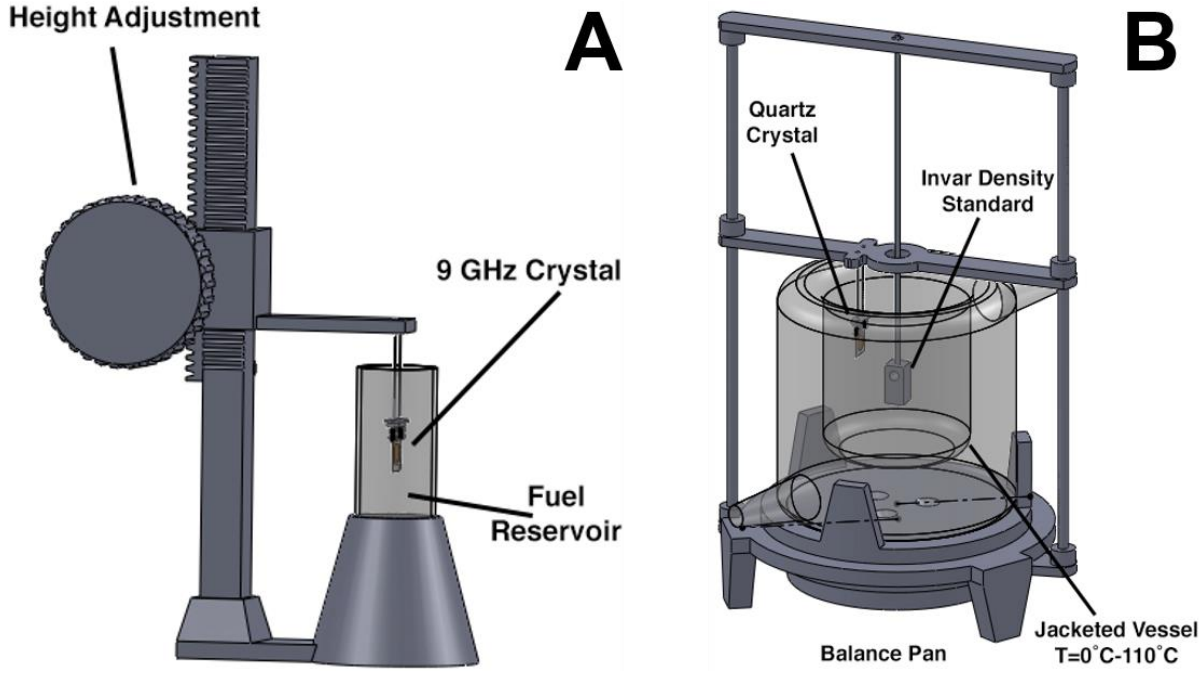

Figure 6: (A) Test fixture for viscosity measurement. (B) Density measurement rig.

A calibration curve of viscosity measurements was found comparing reference mixtures and is shown in Figure 7. Soe of the selected diesel fuels has viscosities outside of the calibration curve determined for the gasoline biofuels. A new calibration curve was generated using mixtures of glycerol and water which have paramaterized density and viscosity equations.

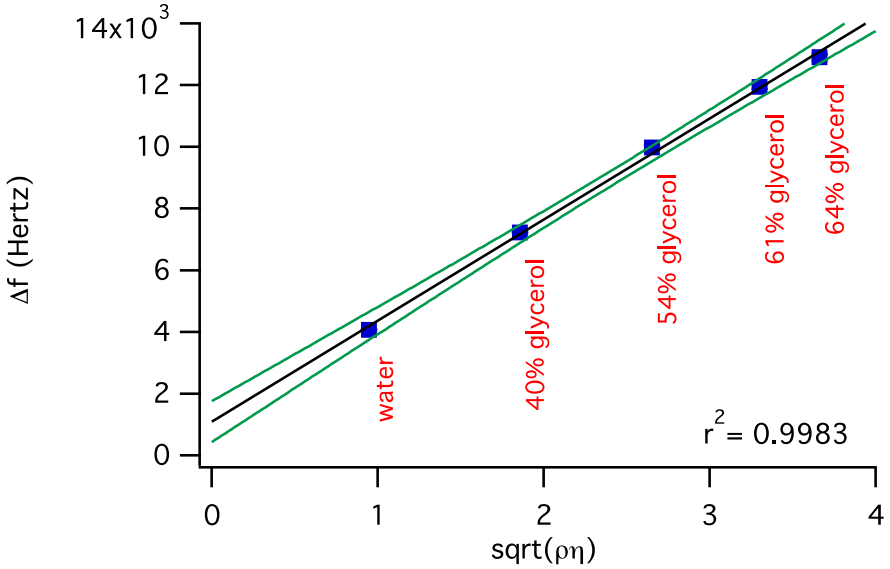

Figure 7: Calibration Curve of viscosity test rig using various mass fraction glycerol/water mixtures.

Results & Discussion

For the fuels tested, the densities and viscosities for neat fuels are presented in Figures 8 and 9, respectively.

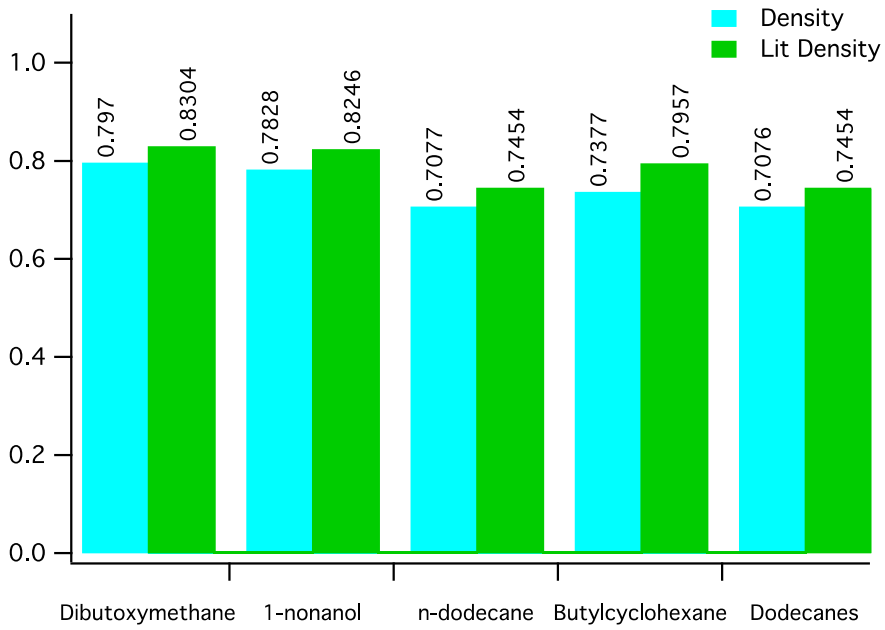

Figure 8: Fuel Densities.

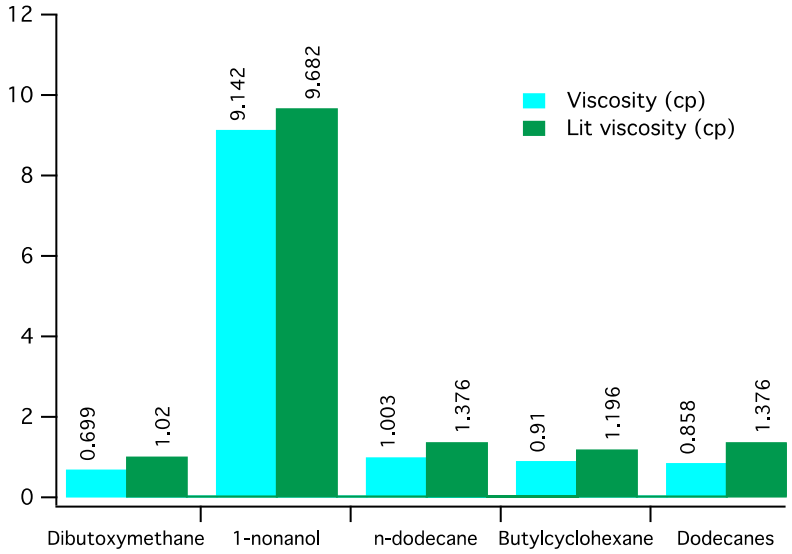

Figure 9: Fuel viscosities at 25± 2 °C.

For the fuels tested, the densities and viscosities for neat fuels are presented in Figures 8 and 9, respectively. Blended data is presented in Table 3.

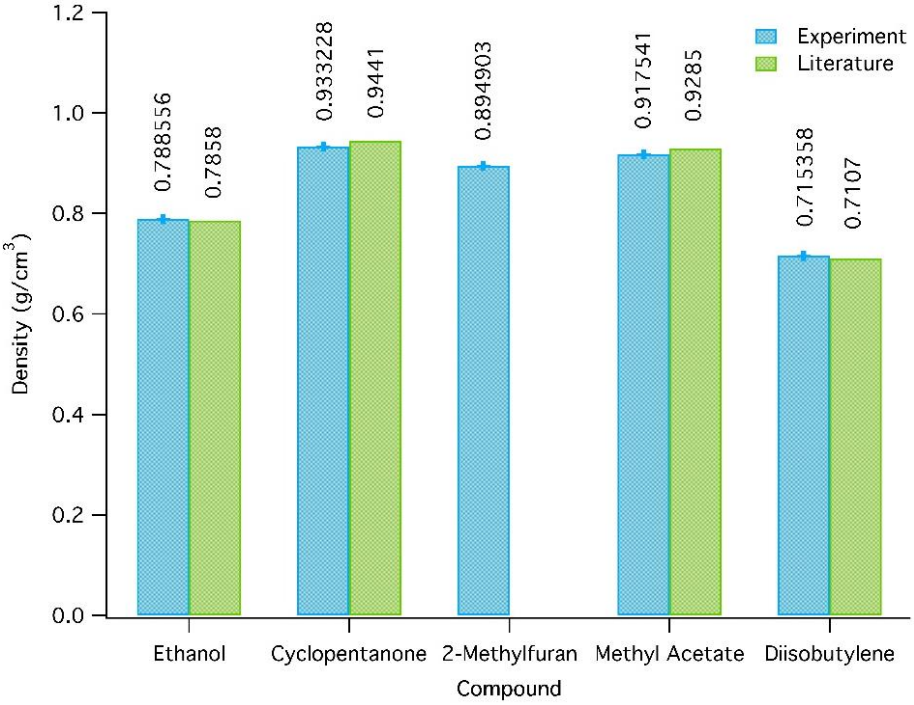

Figure 8: Fuel Densities.

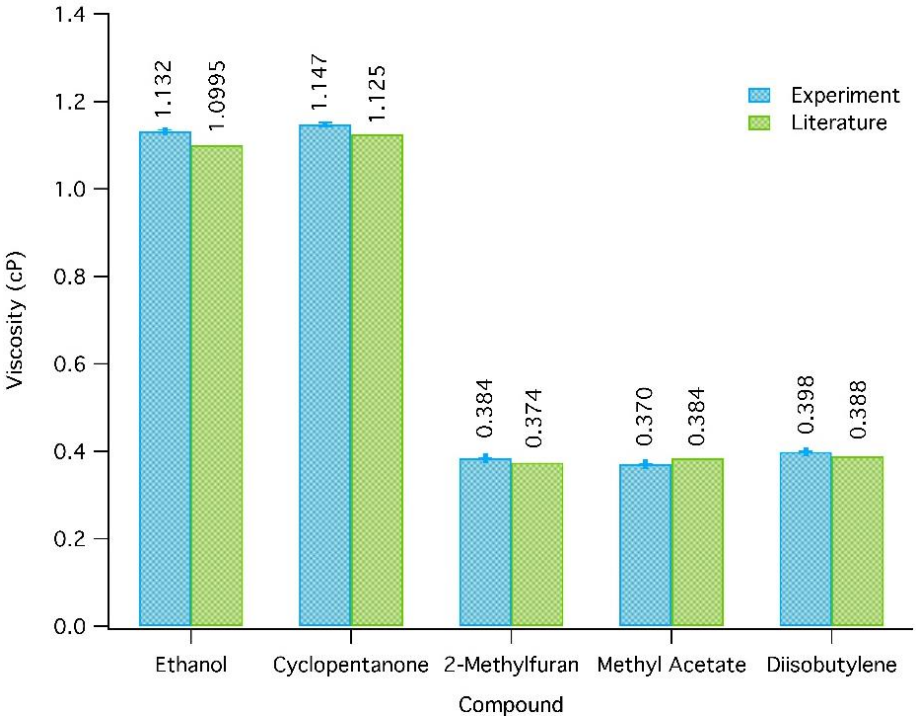

Figure 9: Fuel viscosities at 25± 2 °C.

Table 3: Density and viscosity for mixtures of selected compounds (by volume) and certified 96 RON gasoline.

Compound	Density (g/cm^3)	SD (g/cm^3)	Viscosity (cP)	SD (cP)
1:9 Ethyl Alcohol	0.744 546 012	0.000 227 453	0.413 798 149	0.039 845 255
2:8 Ethyl Alcohol	0.746 344 696	0.000 136 828	0.474 060 038	0.043 051 413
3:7 Ethyl Alcohol	0.750 012 727	0.000 152 302	0.487 595 344	0.047 766 261
1:9 Cyclopentanone	0.763 445 042	0.000 273 576	0.467 560 979	0.043 268 221
2:8 Cyclopentanone	0.777 661 071	0.000 253 208	0.499 303 607	0.045 380 760
3:7 Cyclopentanone	0.791 009 876	0.000 210 904	0.545 256 901	0.048 183 565
1:9 Methyl Acetate	0.800 442 975	0.000 169 191	0.379 030 109	0.039 506 640
2:8 Methyl Acetate	0.778 913 726	0.000 177 217	0.393 467 759	0.039 731 464
3:7 Methyl Acetate	0.783 898 650	0.000 149 568	0.367 980 620	0.038 418 054
1:9 Ethyl Acetate	0.748 721 528	0.000 183 479	0.322 424 885	0.036 459 086
2:8 Ethyl Acetate	0.766 579 892	0.000 353 390	0.407 559 665	0.040 159 606
3:7 Ethyl Acetate	0.778 252 067	0.000 356 023	0.380 198 714	0.038 971 100
1:9 Diisobutylene	0.733 586 886	0.000 173 751	0.370 060 977	0.037 153 596
2:8 Diisobutylene	0.729 231 501	0.000 169 191	0.343 978 818	0.036 649 271
3:7 Diisobutylene	0.724 773 334	0.000 246 867	0.389 816 707	0.037 979 206
1:9 Methyl Furan	0.749 884 249	0.000 305 601	0.362 018 379	0.037 153 786
2:8 Methyl Furan	0.769 457 786	0.000 141 202	0.371 406 143	0.038 219 736
3:7 Methyl Furan	0.778 810 944	0.000 168 161	0.366 945 727	0.038 219 758

Task 2.9 Seal Flexible Fuel Compatibility

Introduction

Exposure of elastomers to biofuels can result in both favorable and unfavorable polymer/biofuel reactions. Aromatic hydrocarbons and oxygenated additives greatly affect the behavior and structure of elastomer seals. Prolonged exposure of elastomers to hydrocarbon fuel can result in changes to o-ring volume and thus other dimensional changes. The extent of these changes is a measure of the elastomer's ability to resist chemical interactions with the fuel. For example, small changes in volume indicate a high resistance (slow chemical reaction) between the elastomer (and filler material) and hydrocarbon compound.

A small amount of swelling is desireable for seal performance, but sizeable volume changes in an o-ring may compromise a seals integrity. With excessive swelling, an overfilled groove will cause seal failure and leakage. Physical property changes are typically accompanied by an increase in volume, meaning the greater the volume change the greater the change in o-ring thickness, diameter, and mass. This study will investigate the swelling characteristics of Viton o-ring seals after continous contact with neat (unblended) biofuel compounds.

Figure 19. *Interactions between o-ring samples, in a single fuel, were reduced by spacing the samples in each test tube with agate beads.*

Experimental Approach

For each fuel compounds, standard metric 2 mm x 3 mm Viton o-rings were submerged in the test fuel. O-rings were threaded onto a thin wire, spaced apart by agaite beads to prevent elastomer contact, and then submerged as a unit (Figure 1). The agate beads and are inert with no fuel or o-ring interactions expected . Either 5 or 10 o-rings were submerged in each test tube, depending on the frequency of data collection. Mass, density, thickness, and diameter measurements of each o-ring were taken prior to submersion, and again in hour increments up to 6 hours, for short-term analysis. For long-term studies, measurements were taken every few days, and time between measurements increased after months of submersion. A single o-ring was removed from the fuel at a time, rinsed briefly in acetone and gently wiped to remove any fuel droplets. It was then placed in a tared weigh bottle and massed on a Mettler AT20 micro-balance with a range from 2 µg to 22 g (Figure 2). If the o-ring experienced gradual evaporation of fuel the first stable mass was recorded.

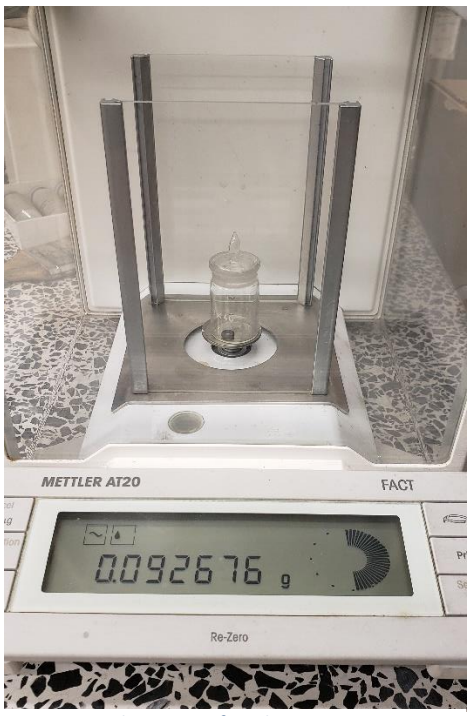

Figure 20. *The mass of each o-ring was measured using a microbalance while the o-ring is enclosed in a glass weigh bottle.*

After the mass measurement, the o-ring was transferred to a Sartorius MC4108 mass balance, containing a scaffold and raised platform designed to measure water-submerged mass (Figure 3). A platform holds a jacketed water bath and stands off the balance to ensure the bath does not contribute to the mass measurement. Within the jacket, coolant flows through an inlet and outlet from a chiller held at 25 °C, maintaining the water bath at roughly room temperature.

A scaffold resting on the balance tray reaches above the bath, holding a hook upon which each o-ring is placed. The balance has a range of 2 µg to 21g, and ±1 ppm/°C sensitivity. This scaffold and hook is tared while some of the hook is submerged at the current water level. Then, the o-ring is placed on the hook, enabling the recorded mass to reflect only the elastomer. After removing from the water bath, the o-ring is dipped briefly in acetone and wiped to remove any traces of moisture. The volume change was then calculated using Equations 1.

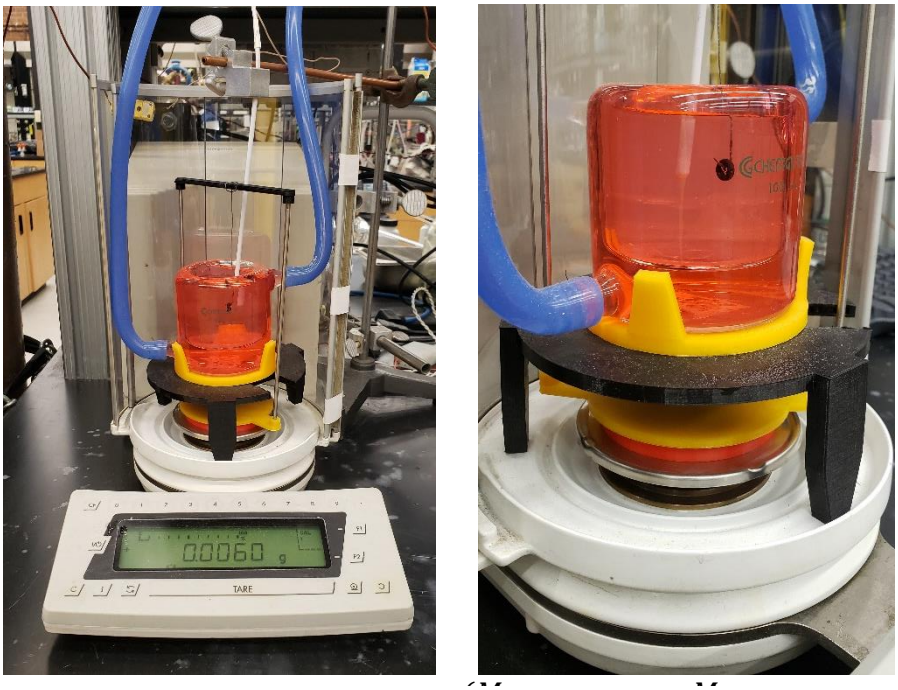

Figure 21. *The density of each o-ring is measured while submerged in distilled water.* $erged)$

Thickness and diameter of the o-rings were determined by a Starrett No. 796XFL-1 digital micrometer with a range of 0 – 25 mm, resolution of 0.001 mm, and an accuracy of ±0.002 mm. Here, any damage to the o-ring is assessed before quickly replacing the o-ring in a new test tube containing the same fuel. Care iwas taken to ensure o-rings remained outside the fuel bath for as little time as possible. While one o-ring is undergoing measurement, the rest are held submerged.

Results and Discussion

Compatibility tests between Viton o-rings and diesel candidate compounds showed minimal volume and mass changesand thus good chemical compatibility. Over a time span of approximately 250 days, variations in mass, volume, and dimention changed within the o-ring were not large. Figures 4 and 5 show these variations over the test time. Overall changes are summarized in Table 1. Two of the fuels, butyl cyclohexane and short term dodecanes, experienced a loss in volume. This phenomena, was observed in the previous experiments with bio-derived jet fuels and indicates that these compounds may produce seal failure if used unblended.[1]

Long-Term Seal Analysis

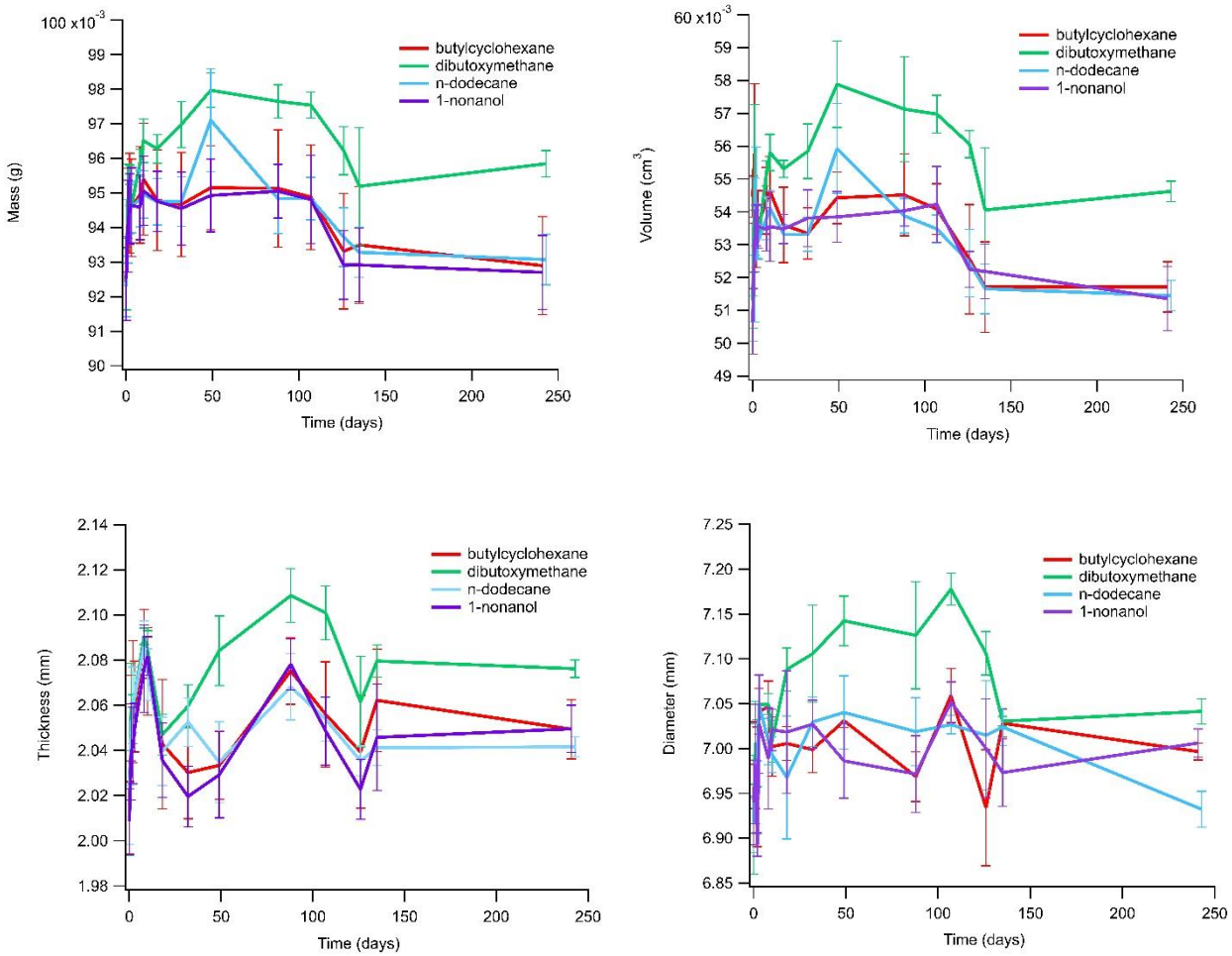

Figure 22. *O-ring variations in mass (top left), volume (top right), thickness (bottom left), and diameter (bottom right) over approximately 240 days shows minimal swelling induced by the fuel.*

Short-Term Seal Analysis

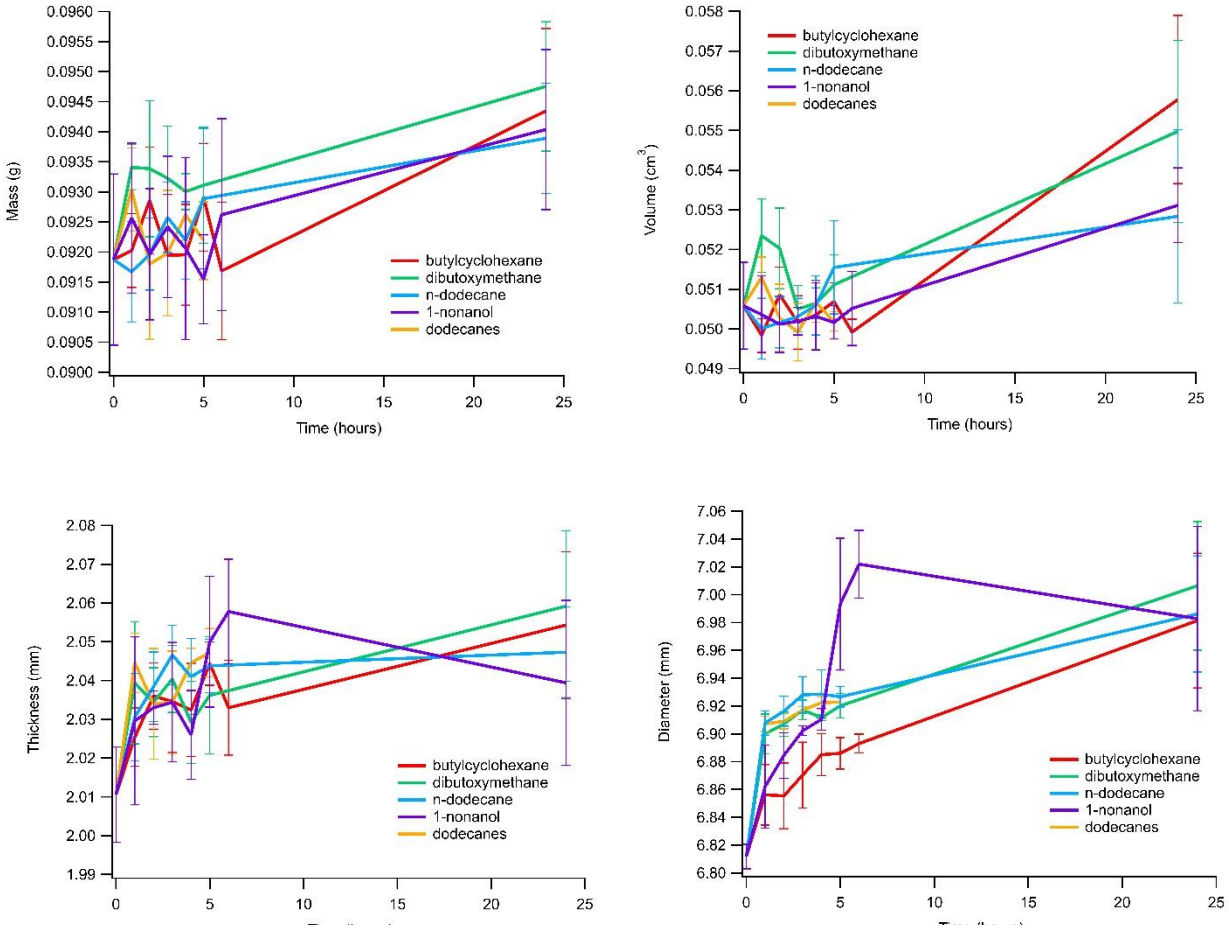

Figure 23. *O-ring variations in mass (top left), volume (top right), thickness (bottom left), and diameter (bottom right) over a shorter time of 24 hours.*

Table 3. Overall changes in mass, volume, thickness, and diameter for each fuel was small.

Fuel	Days	ΔMass	ΔVol	ΔThickness	ΔDiameter
1-nonanol	241	1.80E-04	6.90E-04	4.11E-02	6.64E-02
dibutoxymethane	243	3.34E-03	3.32E-03	6.67E-02	1.15E-01
n-dodecane	243	7.74E-04	6.97E-04	3.02E-02	1.68E-02
butylcyclohexane	241	4.72E-04	-2.75E-03	3.93E-02	5.24E-02
dodecanes	6 hours	3.15E-04	-3.98E-04	3.66E-02	1.11E-01

Post Test	Vol. (cm^3)	Vol. Std. Dev. (%)	Mass (g)	Mass Std. Dev. (%)
2-methylfuran	0.0759	4.87	0.114787	3.19
cyclopentanone	0.1600	2.16	0.194250	1.69
diisobutylene	0.0558	4.42	0.095541	1.46
ethanol	0.0580	7.62	0.098261	3.77
ethyl acetate	0.1685	3.71	0.196642	2.94
methyl acetate	0.1518	2.53	0.191716	1.88

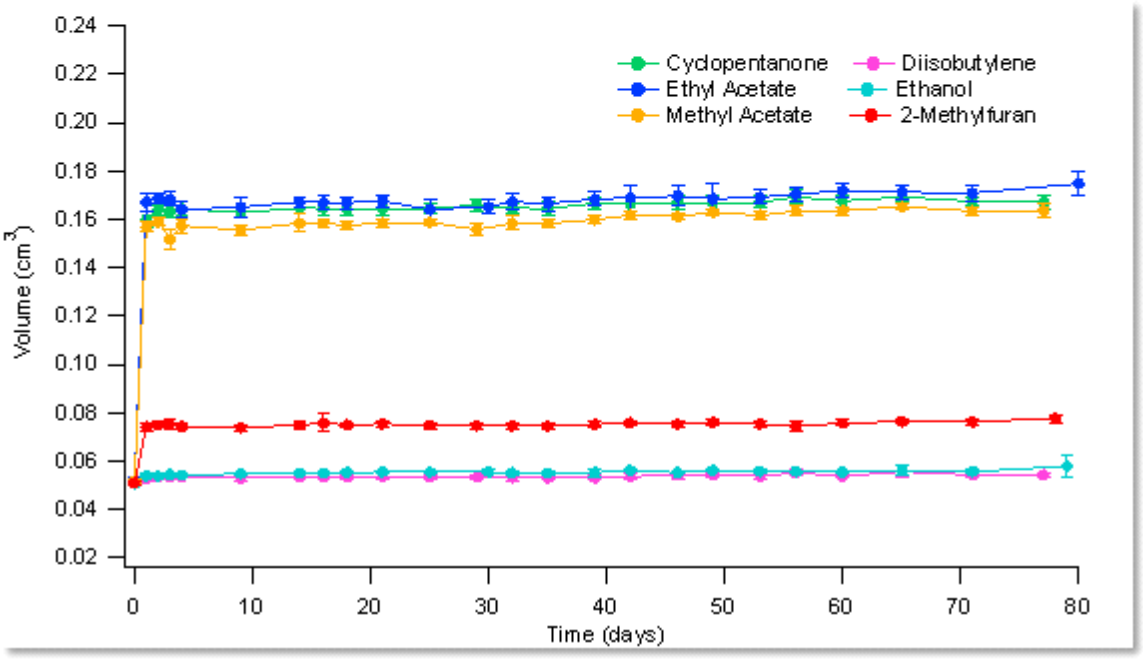

Task 3: Correlation of molecular structure

Biofuels evaluated by UCF were intended to be used as drop-in replacements for conventional gasoline and diesel. Molecular configurations for evaluated fuels are shown below where all hydrocarbons have the same ideal end products of H_2O and CO_2. Of those tested fuels, there are numerous classifications which may be cross represented including: mono--oxygenated, cyclic, and containing vinylic (C=C) bonds. Each of these attributable bond types features a unique bond energy configuration set which dictates subsequent combustion properties.

- **Ethanol (alcohol)**

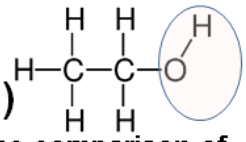

  - **Selected as a baseline comparison of existing biofuels**
- **Methyl Acetate (ester)**

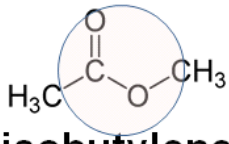

- **Diisobutylene 1 & 2 (alkenes)**

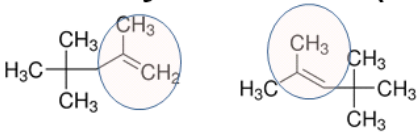

- **Methyl Furan**

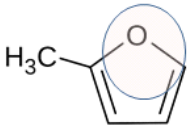

- **Cyclopentanone (ketone)**

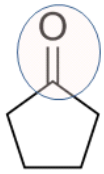

- **The 5 candidates were chosen for their specific functional groups as highlighted in the figures. The correlation of the molecular structures will be beneficial to identify fuel similarities. The goal is to examine the relationship between the experimental results from task 2 and the fuel molecular structure. This information will be useful for the Co-Optima effort for predicting new fuels (outside of the selected ones) and their behavior.**

- Spray Cone Angles and Droplet
  - Increases in the inertial moment of the fuel molecule trend with larger spray cone angles. Furthermore, blending multiple fuels compounds, increases the number of small particles.
- Fuel-Air Flame Measurements
  - Alcohols and furans have lower fuel-air equivalence ratio (close to stoiciometric) under comparable conditions than esters, ketones, and alkenes. Thus for SI engines, optimal burning could be achived with alcohols and furans.
  - No remarkable differences between alcohols, and furans when it comes to fuel-air flame burning.
- Carbon Deposition
  - Prevalence of C-C and C=C, versus C-O or C=O bonds increases the quantity of soot deposited.
- Viscosity & Density
  - The existence of a C=C bond exhibits a shorter bond length than a C-C bond, thus the orbital dipole nature of this compound is decreased resulting in reduced viscosity.

- Density is dependent on both molecular weight and dipole characteristics of molecular structure.

- Laminar Burning Velocity
  - Alcohols, ketones, and furans have higher laminar burning velocities under comparable conditions than esters and alkenes. Thus for SI engines, where flame speeds are a design parameter, alkenes and esters may not be a good choice.
  - No remarkable differences between alcohols, ketones, and furans when it comes to flame speeds.
- Synchrotron Photoionization
  - Position of a C=C double bond can greatly impact the ability of a fuel to ignite. As it can be seen the ignition temperature of DIB2 which has a C=C bond on the backbone, is significantly below that of DIB1 which has a C=C bond on a side chain.
- Distillation
  - The larger the hydrocarbon chain backbone, or the existence of a ring structure, increases retention time.
  - The addition of functional groups lowers the retention time of a fuel.
- Fuel Swell
  - The addition of non-alcohol functional groups and ring chemistry greatly enhance the ability of Viton to uptake compounds.
  - Compatibility best for alcohols and alkenes, worst for ketones and acetates
  - Straight chain hydrocarbons exhibit the least amount of swelling in seals.
- Soot Formation
  - Ethanol which has the shortest carbon chain of any species tested and is oxygenated produces the least amount of soot at the highest sooting condition tested.
  - Subsequent lowest sooting species: cyclopentanone and methyl acetate are both oxygenated hydrocarbons which do not feature a C=C bond.
  - Methyl furan, and DIB produced the most soot of all fuels tested. Both compounds are unsaturated (have the C=C structure) and thus such compounds will make more soot. However, the fact that methyl furan produces less soot compared to DIB is due to the presence of an oxygen within the parent fuel (greatly inhibits soot formation.)

For species which have the vinylic bonds and no other associated features, a lower laminar burning velocity is observed which is presumed to correspond to a lower overall reaction rate. These difficulties are associated with the energy barrier associated with breaking the C=C bond which can either become CO_2 or become soot precursors. For oxygenated species, initiation reactions have the chance to produce a radical pool with oxygenated intermediates; these species will typically have reduced soot forming tendency as the breakdown products inherently have a higher C:O ratio. Conversely for polyoxygenated species such as methyl acetate, there is a reduction in reaction rate and higher than expected soot forming tendency even though there is a large oxygen content. This is assumed to be the result of low exothermicity in reactions It can be seen that species which are both mono-oxygenated and cyclic feature higher LBVs than other evaluated species. Two primary factors are identified which contribute to these phenomena.

Table: Cross Referenced comparison of investigated biofuel species.							
Compound	**Mono-oxygenate**	**Cyclic**	**Vinylic**	**Compound**	**Mono-oxygenate**	**Cyclic**	**Vinylic**
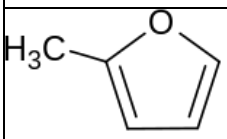 2-Methyl Furan	✓	✓	✓	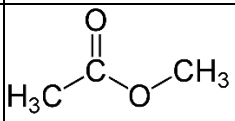 Methyl Acetate			
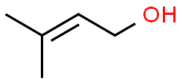 Prenol	✓		✓	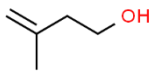 Iso-prenol	✓		✓
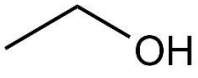 Ethanol	✓			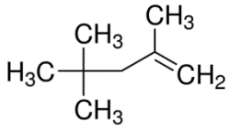 α-Diisobutylyene			✓
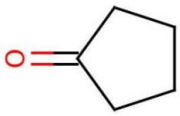 Cyclopentanone	✓	✓		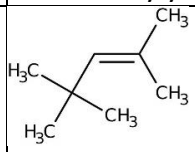 β-Diisobutylyene			✓

Patents: No new patents have been filed.

Publications / Presentations:

1. Reyes, Jonathan, Ranjith Kumar Abhinavam Kailasanathan, and Kareem Ahmed. "Relationship between the Chemiluminescence Intensity Ratio of C2* and CH*, Charge Pressure, and Equivalence Ratio for Gasoline." Energy & Fuels 32, no. 10 (2018): 10933-10940.

2. Salauddin, S., Reyes, J., Kumar, R., AHMED, K.A., “Spray and Fuel-Air Characterization of Advanced Biofuels,” 2020 AIAA Aerospace Sciences Meeting, 2020.

3. Barak, Samuel, Ramees K. Rahman, Sneha Neupane, Erik Ninnemann, Farhan Arafin, Andrew Laich, Anthony C. Terracciano, and Subith S. Vasu. "Measuring the effectiveness of high-performance Co-Optima biofuels on suppressing soot formation at high temperature." Proceedings of the National Academy of Sciences 117, no. 7 (2020): 3451-3460.

4. Arafin, Farhan, Andrew Laich, Erik Ninnemann, Robert Greene, Ramees K. Rahman, and Subith S. Vasu. "Influence of the double bond position in combustion

chemistry of methyl butene isomers: A shock tube and laser absorption study." *International Journal of Chemical Kinetics* (2020).

5. Kim, Gihun, Anthony Terracciano, Subith Vasu, and Bader Almansour. *High-Pressure Laminar Burning Velocity Measurements of Ethanol-A Co-Optima Fuel Candidate*. No. 2020-01-0332. SAE Technical Paper, 2020.

6. Dong, Xiaorui, Erik Ninnemann, Duminda S. Ranasinghe, Andrew Laich, Robert Greene, Subith S. Vasu, and William H. Green. "Revealing the critical role of radical-involved pathways in high temperature cyclopentanone pyrolysis." *Combustion and Flame* 216 (2020): 280-292.

7. Neupane, S., Rahman, R.K., Baker, J., Arafin, F., Ninnemann, E., Thurmond, K., Wang, C.H., Masunov, A.E. and Vasu, S.S., 2020. DMMP pyrolysis and oxidation studies at high temperature inside a shock tube using laser absorption measurements of CO. *Combustion and Flame*, *214*, pp.14-24.

References

[1] B. Almansour, S. Alawadhi, S. Vasu, Laminar Burning Velocity Measurements in DIPK-An Advanced Biofuel, SAE Int. J. Fuels Lubr. 10 (2017).